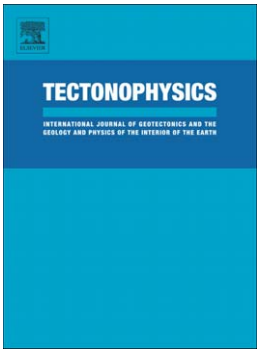

Geophysical anomalies and quartz deformation of the Warburton West structure, central Australia

A.Y. Glikson, A.J. Meixner, B. Radke, I.T. Uysal, E. Saygin, J. Vickers, T.P. Mernagh

PII: S0040-1951(14)00647-7
DOI: doi: 10.1016/j.tecto.2014.12.010
Reference: TECTO 126501

To appear in: *Tectonophysics*

Received date: 22 September 2013
Revised date: 12 December 2014
Accepted date: 18 December 2014

Please cite this article as: Glikson, A.Y., Meixner, A.J., Radke, B., Uysal, I.T., Saygin, E., Vickers, J., Mernagh, T.P., Geophysical anomalies and quartz deformation of the Warburton West structure, central Australia, *Tectonophysics* (2015), doi: 10.1016/j.tecto.2014.12.010

Geophysical anomalies and quartz deformation of the Warburton West structure, central Australia

A.Y. Glikson[1, 2], A.J. Meixner[2], B. Radke[2], I.T. Uysal[4], E. Saygin[3], J. Vickers[3] T.P. Mernagh[2]

1. Australian National University and Geothermal Energy Centre of Excellence, University of Queensland.
2. Geoscience Australia.
3. Research School of Earth Science, Australian National University
4. Geothermal Energy Centre of Excellence, University of Queensland.

Abstract

This paper reports geophysical anomalies and intra-crystalline quartz lamellae in drill cores from the Warburton West Basin overlapping the border of South Australia and the Northern Territory. The pre-Upper Carboniferous ~450x300 km-large Warburton Basin, north-eastern South Australia, is marked by distinct eastern and western magnetic, gravity and low-velocity seismic tomography anomalies. Quartz grains from arenite core samples contain intra-crystalline lamellae in carbonate-quartz veins and in clastic grains, similar to those reported earlier from arenites, volcanic rocks and granites from the Warburton East Basin. Universal stage measurements of quartz lamellae in both sub-basins define Miller-Bravais indices of {10-12} and {10-13}. In-situ quartz lamellae occur only in pre-late Carboniferous rocks whereas lamellae-bearing clastic quartz grains occur in both pre-late Carboniferous and post –late Carboniferous rocks – the latter likely redeposited from the pre-late Carboniferous basement. Quartz lamellae in clastic quartz grains are mostly curved and bent either due to tectonic deformation or to re-deformation of impact-generated planar features during crustal rebound or/and post-impact tectonic deformation. Seismic tomography low-velocity anomalies in both West and East Warburton Basin suggest fracturing of the crust to depths of more than 20 km. Geophysical modelling of the Cooper Basin, which overlies the eastern Warburton East Basin, suggests existence of a body of high-density (~2.9—-3.0 gr/cm^3) and high magnetic susceptibility (SI ~ 0.012-0.037) at depth of ~6-10 km at the centre of the anomalies. In the Warburton West Basin a large magnetic body of SI = 0.030 is modelled below ~10 km, with a large positive gravity anomaly offset to the north of the magnetic anomaly. In both the Warburton East and Warburton West the deep crustal fracturing

suggested by the low velocity seismic tomography complicates interpretations of the gravity data. Universal Stage measurements of quartz lamellae suggest presence of both planar deformation features of shock metamorphic derivation and deformed planar lamella. The latter may be attributed either to re-deformation of impact-generated lamella, impact rebound deformation or/and post impact tectonic deformation. The magnetic anomalies in the Warburton East and West sub-basins are interpreted in terms of (1) presence of deep seated central mafic bodies; (2) deep crustal fracturing and (3) removal of Devonian and Carboniferous strata associated with rebound of a central uplift consequent on large asteroid impact. Further tests of the Warburton structures require deep crustal seismic transects.

Introduction

The discovery of large impact structures, including Vredefort (South Africa; 298 km; 2023 ± 4 Ma) (Dietz, 1961; Kamo et al., 1996; Therriault et al., 1997), Sudbury (Ontario; 250 km; 1850 ± 3 Ma) (Dietz, 1964), Chicxulub (Mexico; 170 km; 64.98 ± 0.05 Ma; Hildebrand et al., 1991), Manicouagan (Quebec; 214±1; 85 km; Dressler, 1990), Woodleigh (Western Australia; 120 km; 360 Ma; Mory et al., 2000; Glikson et al., 2005; Uysal et al., 2005), Popigai (Siberia; 90 km, 35.7 ± 0.2; Masaitis, 1998); Chesapeake Bay (off-shore Virginia; 85 km; 35.5 ± 0.3 Ma; Poag et al., 2004), Morokweng (South Africa; 70 km; 145.0±0.8; Hart et al., 2000 (for further details refer to the Earth Impact Database, 2001, and Glikson, 2013) underpins the significance of large asteroid impacts in the history of Earth. The development of geophysical exploration and drilling techniques uncovered a number of large buried impact structures identified by circular gravity, magnetic and seismic tomography anomalies and confirmed by shock metamorphic features. In Australia such discoveries include Woodleigh, Tookoonooka (Eromanga Basin, Queensland - 55-65 km; ~125 Ma; Gorter et al., 1989; Gostin and Therriault 1997), Acraman (Gawler Plateau, 90 km, 580 Ma; Gostin et al., 1986; Williams, 1994), Talundilly (Eromanga Basin, Queensland - 84 km, 125 Ma; Longley 1989; Gorter and Glikson, 2012), and probable impact structures (Gnargoo, north Carnarvon Basin, Western Australia; Iasky et al., 2001; Iasky and Glikson, 2005), and Mount Ashmore (Timor Sea; Glikson et al., 2010). Very large impact structures yet to be confirmed include the ~500 km-large Otish Basin, Quebec, containing intra-crystalline planar deformation features in quartz and cored by a mafic body (Genest et al., 2011). The identification of impact structures depends critically on microstructural criteria of shock metamorphism (Carter, 1965, 1968; Carter and Friedman, 1965; Carter et al., 1986; Alexopoulos et al., 1988; Lyons et al., 1993; Grieve et al., 1996; Stöffler and Langenhorst, 1994; Engelhardt et al., 1969; Vernooij and Langenhorst, 2005; Spray and Trepmann, 2006;

Ferriere et al., 2009; French and Koeberl, 2010; Hamers and Drury, 2011; Glikson and Uysal, 2013).

Duane and Reimold (1990) suggested the existence of a ~800 km-large impact structure under the Simpson Desert, South Australia and Northern Territory. The Warburton Basin in South Australia, with extensions into Queensland and Northern Territory, underlies an area approximately ~400,000 km^2 (Figure 1) consisting of a >4.5 km thick sequence including a basal suite of felsic volcanic rocks overlain by late Cambrian carbonates and Ordovician pelagic to shelf clastic sediments (Gatehouse et al., 1995; Gravestock and Gatehouse, 1995; Radke, 2009; Roberts et al., 1990; Sun, 1997, 1998, 1999; Sun et al., 1994). Studies of the Warburton East Basin have identified intra-crystalline planar lamellae in quartz grains within granites, sediments and volcanic rocks in drill cores over an area ~220×195 km-large between Walkillie-1 in the north, Cutapirrie-1 in the south, Kalladeina-1, and Jennet-1 in the west (Glikson and Uysal, 2010; Glikson et al., 2013). The present paper reports the identification of intra-crystalline lamellae in quartz in drill cores in the Warburton West Basin and the significance of major magnetic, gravity and seismic tomography anomalies of the Warburton West and Warburton East Basins.

Nomenclature

In this paper references to intra-crystalline lamellae in quartz are made in the following ways: (1) descriptive text references are made in non-genetic terms, mainly as "intra-crystalline quartz lamellae" or "quartz lamellae"; (2) Where interpretations of intra-crystalline quartz lamellae are discussed the terms "Planar Features" (PF), "Planar Deformation Features" (PDF) and "Metamorphic Deformation lamellae", reference is made to definition of these planar features as discussed by French (1998) and French and Koeberl (2010).

Geological Methods

Drill hole cores and cuttings were sampled from 6 drill holes located in the Simpson Desert straddling the South Australia–Northern Territory border (Figure 1b), including the Macumba-1 (2 samples), Mokari-1 (4 samples), Pandieburra-1 (3 samples), Purni-1 (5 samples), Walkandi-1 (8 samples), Witcherie-1 (9 samples) (Table 1). Samples were collected from stratigraphic levels within the pre-late Carboniferous Warburton Basin as well as from post-Carboniferous units (Mokari-1, Purni-1) (Table 1). The rocks include fine-grained to medium-grained quartzite, quartz-feldspar arenite, feldspathic arenite, feldspathic greywacke, siltstone, carbonated siltstone and carbonated siltstone, including carbonate-

quartz veins. All samples were studied in thin section in a search for intra-crystalline quartz lamellae. Intra-crystalline quartz lamellae are observed in (A) detrital quartz grains in arenites; (B) quartz-carbonate veins (Walkandi-1 3122.9 m) (Table 1). The best formed intra-crystalline quartz lamellae are observed in quartz-carbonate veins and irregular aggregates injected into foliated siltstone of Walkandi-1 3229.1 m core samples (Figure 5a). The rock consists of laminated to weakly cleaved siltstone consisting of aphanitic cryptocrystalline quartz-clay aggregates pervaded by veinlets and irregular granular aggregates of microcrystalline to fine-grained quartz and carbonate (Figure 5a [a and b]). By contrast penetrative intra-crystalline quartz lamellae which occur in fine to medium grained detrital quartz grains in arenites range from planar to curved and bent (Figures 3, 4 and 5).

The crystal orientations of intra-crystalline quartz lamellae were measured using a 4-axis U-stage Leitz microscope (magnification ×120) (Stöffler and Langenhorst, 1994). The analysis is complicated by the relatively small proportion of planar sets-bearing quartz grains in most samples, where only one grain in many hundreds of grains displays intra-crystalline lamellae. The restriction of lamellae to sectors within the grains (Figures 5c, d) and their commonly wavy and clouded nature of (Figures 5a, b) required selection of least-bent lamellae for measurement. In general deformed quartz lamellae occur in single sets and less commonly in intersecting planar sets (Figure 5a, b). Measurements are complicated where wavy orientations of lamellae complicate measurements, which results in errors in the definition of the C optic axis and planar traces within the host quartz grains. For these reasons in each case the orientations of the optic axis ($C_{OA}Qz$) and of the orientation of quartz lamellae relative to C_{OA} were derived from the mean of 3 measurements of the angle between $C_{OA}Qz$ and the pole to lamellae ($C_{OA}Qz \wedge P_{PE}$), recorded on a Wulff stereogram (Engelhardt and Bertsch, 1969). Frequency distribution of $C_{OA}Qz \wedge P_{PE}$ angles are plotted in Figure 6. Frequency plots include multiple intra-grain measurements as well as measurements of individual planar sets. Errors arising from the bent and wavy geometry of lamellae and errors in readings of the C optic axis and vertical positioning of quartz lamellae ($C_{OA} \wedge P_{PE}$) are estimated as ± 3°.

Geophysical Methods

Seismic tomography images which record the ambient crustal seismic velocity at different levels of the crust, as applied in the US (Shapiro et al., 2005), South Korea (Kang and Shin, 2006); Europe (Yang et al., 2007; Stehly et al., 2009) and Australia (Saygin and Kennett, 2010, 2012), allow cross-correlations of simultaneously recorded seismic ambient noise at two different stations and the extraction of the 'Green's Function' - a wavelet allowing information from the medium along the connecting path of the two stations. Systematic cross-

correlations between the different stations of a seismic network allows measurements of the travel time variations between each station pair, used in a tomographic inversion method to map variations of the seismic velocities for regions covered by the network. Studies of the ambient seismic noise tomography of the Australian continent indicate close spatial correspondence between the features of the group wavespeed anomaly map and major geological features (Saygin and Kennett, 2010, 2012). Tomographic imaging of the ambient seismic noise cross-correlations delineates Rayleigh type surface wave group velocity variation maps from the Low wavespeeds, suggesting correlation with the thickness of sedimentary cover as well as thermal anomalies. Anomalies imaged with shorter period surface waves are mostly associated with thick sedimentary sequences. At the longer periods reduced wavespeeds are most likely caused by the elevated temperatures. A correlation between major low velocity tomography anomalies and the Woodleigh impact structure and Warburton East shock metamorphosed structure suggests that in these terrains deep crustal fracturing constitute a major factor for such anomalies (Glikson et al., 2013).

The Total Magnetic Intensity (TMI) data used in the investigation of the Warburton Basin are based on an airborne magnetic survey conducted for Geoscience Australia by UTS Geophysics Pty Ltd along N-S 400 meters-spaced lines at an above-ground elevation of 60 meters (Geoscience Australia, 2009). A distinct magnetic anomaly can be modelled coincident with the centre of Warburton West body with similar magnetic susceptibility values (SI) values as for the Warburton East Basin (Meixner et al., 2000) with a large depth extent body of moderately high SI. The irregular shaped outline of the body is based on the anomaly as imaged in the first vertical derivative. The gravity data are based on an airborne survey conducted for Geoscience Australia by Daishsat Geodetic Surveys with station spacing of 4.0X4.0 km (Geoscience Australia, 2007). An E-W section suggests the magnetic anomaly is coincident with a gravity anomaly that can be modelled using a density contrast of 0.1 g/cm^3, i.e. a 2.9 g/cm^3 for body within a 2.8 g/cm^3 background similar to the Warburton East model, supporting a modelled mafic intrusion in depth. By contrast a north-south section indicates no gravity anomaly coincident with the magnetic body (see below).

Warburton East Basin

The Warburton East Basin (Figure 1a and b), including sediments and volcanics intruded by the Big Lake Granite suite, has been deformed and uplifted during the Carboniferous Alice Springs Orogeny and buried beneath the Cooper Basin (Gravestock et al., 1998; Sun et al., 1994; Sun, 1998, 1999; Radke, 2009). Structural orientations range from sub-horizontal below the Patchawarra Trough and Gidgealpa–Merrimelia–Innamincka Ridge to vertical and

locally overturned. Early to Middle Carboniferous granitic intrusives of the Big Lake Suite resulted in local contact metamorphism of Cambrian rocks below the Nappamerri Trough. The basal unconformity separating the Upper Palaeozoic Cooper Basin from the Lower Palaeozoic Warburton Basin is associated with a <150 meters-thick weathered zone. Several older disconformities representing tectonic events occur in the Lower Palaeozoic, including events representing sea-level fall and development of karst. Early Ordovician stratigraphy indicates development of major delta on the northern margin of a deep marine trough. During the Early to Late Cambrian intra-plate rifting propagated north-northwest. The Devonian-Carboniferous Alice Springs orogeny resulted in arcuate NE tectonic trends (Radke, 2009).

The Warburton East Basin is associated with major geophysical anomalies which include a positive magnetic high of near-200 nT centred on a ~25 km-wide magnetic low of <100 nT which has been modelled in terms of a magmatic body deeper than 6 km (Meixner et al., 1999, 2000). A distinct seismic tomographic low velocity anomaly may reflect its thick (9.5 km) sedimentary section, high temperatures and possible deep fracturing to mid-crustal depth (Saygin and Kennett, 2010, 2012; Glikson et al., 2013). Scanning electron microscope (SEM) analyses of granites resolves microbreccia veins consisting of micron-scale particles injected into resorbed quartz grains and likely representing recrystallized pseudotachylite (Glikson and Uysal, 2010; Glikson et al., 2013). Intra-crystalline planar and sub-planar lamellae in quartz grains have been identified in drill holes in granites, volcanics and sediments over an area >30,000 km^2-large. Intra-crystalline micro-structures in quartz include multiple intersecting planar to curved lamellae, including relic lamellae less than 2 μm wide with spacing of 4–5 μm (Glikson et al., 2013). The lamellae are commonly re-deformed, displaying bent and wavy patterns accompanied with fluid inclusions.

Universal-stage measurements of a total of 243 planar sets in 157 quartz grains indicate dominance of Π{10–12}, ω{10–13} and subsidiary ξ{11–22}, {22–41}, m{10–11} and x{51–61} planes (Fig. 6a), consistent with shock levels of >20 GPa (Stöffler and Langenhorst, 1994; Grieve et al., 1996; French, 1998; Langenhorst, 2002; Vernooij and Langenhorst, 2005; French and Koeberl, 2010). Transmission Electron Microscopy (TEM) analysis displays relic narrow ≤1 μm-wide lamellae which are not regarded as sub grain boundaries and where crystal segments maintain optical continuity, indicating they are not Boehm lamellae. Extensive sericite alteration of feldspar suggests hydrothermal alteration to a depth of ~500 m below the unconformity which overlies the Warburton East Basin (Boucher, 2001; Middleton et al., 2013, 2014). Deformed quartz lamellae are compared to re-deformed planar deformation features in the Sudbury, Vredefort, Manicouagan and Charlevoix impact structures. A 4–5 km uplift of the Big Lake Granite Suite during ~298–

295 Ma (Gatehouse al., 1995) is consistent with missing of upper Ordovician, Devonian and lower to middle Carboniferous strata and possible impact rebound (Glikson et al., 2013)

Warburton West Basin

The Warburton Basin forms a vast subsurface depository where sediments of Cambrian and Ordovician age were deposited in a foreland rift/sag setting north and northeast of the Gawler Craton (Radke, 2009). The supracrustal package comprises basal rift-related volcanics covered by shelf carbonates, and a thick upper package of slope and basinal siliceous clastics. West of the Birdsville Track Ridge, a Proterozoic structure that has been repeatedly active in uplift, is a region that has experienced intermittent subsidence from Devonian through Mesozoic to the Cenozoic. This region has superposed depocentres of the Carboniferous Pedirka Basin, Triassic Simpson Basin, Poolowanna Trough within the Jurassic-Cretaceous Eromanga Basin, and the Cenozoic Lake Eyre Basin. Subsidence is still active. It is less certain that Devonian strata in this region were extensive. These have only been confirmed beneath the Pedirka Basin (Figure 1b), and are inferred from seismic data in the Boorthanna Trough. Late Carboniferous and younger strata completely cover the Warburton Basin (Radke, 2009).

The supracrustal sequences of the Warburton West Basin are of medium to low thickness relative to parts of the Cooper Basin and parts of the Georgina Basin and Amadeus Basin (Figure 4) which contain stratigraphic equivalents of the Warburton Basin. Drill holes reach depths of approximately 3000 meters, intersecting Ordovician, Cambrian and Neoproterozoic units (Table 1). Stratigraphic holes drilled in the Poolowanna, Pandi-Pandi, Dalhausie, Noolyeana and Gason 1:250,000 sheet areas indicate major stratigraphic gaps (lacuna) between Mesozoic, upper Palaeozoic and lower Palaeozoic sequences, consistent with deformation events documented by Radke (2009, Table 1). Units of the Triassic-Jurassic-Cretaceous Eromanga Basin or units of the mainly Permian Cooper Basin overlie Cambrian-Ordovician units of the Warburton Basin or Proterozoic units through major unconformities and paraconformities (Figure 1b) (Veevers, 2009). Drill holes west of the main Warburton West anomaly (Witcherrie-1, Mt Hammersley-1, Dalhausie 1:250,000 sheet) intersect Devonian and Ordovician units (Figure 1b).

The Warburton West Basin and the overlying Pedirka and Simpson Basins are marked by overlapping to part-overlapping major geophysical anomalies >200 km diameter, displaying remarkable similarities to those of the Warburton East Basin (Figures 2a, b, c; 3). These features include:

1. An airborne magnetic anomaly) spanning an area of approximately 8000 km^2 over the Warburton West Basin and the Pedirka Basin and straddling the Northern Territory – South Australia border (~138°00–139°40'E; 25°20' - 26°20'S) (Figure 2a1 and 2b2).
2. A positive Bouguer gravity anomaly (Figure 2b2).
3. A distinct circular low velocity seismic tomography anomaly (~136–140°E; 24 – 28°S) (Figure 3).

The north-eastern part of South Australia includes two of the sharpest low velocity anomalies of the Australian continent, over the Warburton East Basin and over the Warburton West Basin (Figure 3), separated from each other by the Birdsville Track structural ridge. Strong low velocity anomalies pertain to a short seismic period of up to 8.3 s whereas somewhat weaker anomalies pertain to the 12.5 s period, which emphasizes the role of the combined ~9.5 km-thick sedimentary pile of the Eromanga–Cooper–Warburton basins (Radke, 2009). It is suggested that the twin tomographic low velocity anomalies of the Warburton Basin may represent deep crustal fracturing, consistent with an impact origin of the Warburton East structure (Glikson et al., 2013). A temperature profile at 5 km depth (Somerville et al., 1994) indicates high-temperature extending over large regions in northeast South Australia, northwest New South Wales and western Queensland.

Modelling of magnetic and gravity data for the Warburton West Basin indicates that the magnetic anomaly can be reproduced by including a moderately high magnetic susceptibility body (0.033 SI) that has a large depth extent (10,000 m), where the top of the body is at ~10 km depth (Figures 2c). The irregular shaped outline of the magnetic body is based on the extents of the anomaly as imaged in the first vertical derivative (Figure 2b1). The magnitude of the anomaly and hence the modelled geometry are, therefore, similar to the Warburton East body which ranges up to 0.037 SI (Meixner 1999, 2000). There is, however, no distinct gravity anomaly that coincides with the magnetic high. The gravity field in this region is anomalously high in a broad area to the north and also south and west of the magnetic anomaly (Figure 2b2). There are gravity lows consisting of a small circular low located on the western edge of the magnetic high and a larger gravity low to the east of the magnetic high (compare 2b1 with 2b2). These localised gravity lows give the impression of a coincident gravity high with the magnetic high in the east-west modelled section (Figure 2c). Although it is possible to reproduce the east-west gravity profile using a density contrast of 0.1 g/cm^3, i.e. for a 2.9 gr/cm^3 set in a 2.8 gr/cm^3 background, as for the Warburton East model (Meixner, 1999, 2000), no distinct coincident gravity anomaly is observed in the north-south section. The role of deep crustal fracturing, suggested by the seismic tomography

anomalies was not included in the gravity modelling. As numerous similar magnetic anomalies occur across the central Australian region, the geophysical anomalies are not in themselves diagnostic of an impact model.

Intra-crystalline quartz lamellae in the Warburton West Basin

The similarities between the geophysical anomalies of the Warburton West Basin and the Warburton East Basin probable impact structure (Glikson and Uysal, 2010; Glikson et al., 2013) have warranted examination of drill cores from the Warburton West Basin in a search for possible quartz microstructures. Sampling of 31 core cuttings from the Macumba-1, Mokari-1, Pandieburra-1, Purni-1, Walkandie-1 and Witcherrie-1 drill holes included fine grained arenite, quartz arenite, greywacke, carbonate-rich arenites, siltstone and carbonate-rich siltstone (Table 1). Of these core samples 24 samples are from pre-upper Carboniferous age and 7 samples are from post-upper Carboniferous sediments (Table 1) which overlie the Z-unconformity (Boucher, 2001).

Intra-crystalline planar lamellae in quartz grains have been identified in the Walkandi-1, Witcherri-1, Mokari-1 and Purni-1 cores, as follows:

1. Multiple intersecting closely spaced (<4 μm spacing) intra-crystalline lamellae sets occur in quartz grains in quartz-carbonate veins in the Walkandi-1 core (Adelaidean – 3122.9 m) as well as in detrital quartz gains (3068.2 m, 3067.4 m, 2846.9 m) (Figures 5a and 5b).
2. Deformed intra-crystalline lamellae are also present in detrital quartz grains in Walkandi-1 (Figure 5c),
3. Deformed intra-crystalline lamellae occur in detrital quartz grains in Witcherrie-1 (Figure 5c), Purni-1 and Mokari-1 (Figure 5d).
4. Intra-crystalline planar lamellae in quartz grains occur in post Z-unconformity (post late Carboniferous) rocks, including arenites from Walkandi-1 (1461.9m), Purni-1 (1773.4 m, 1773.7 m) and Mokari-1 (2031.3 m) (Figure 1b). These quartz grains could have been redeposited from shocked early Palaeozoic rocks.

Evidence for the origin of quartz lamellae in the Warburton East Basin includes:

1. Correspondence between measured CO_{AQ} ^ $P_{LAMELLA}$ angles and Miller-Bravais indices, mainly ω{10–13} and Π{10–12} (Figure 6a, b), correlated with shock levels higher than >20 GPa (French, 1998; Langenhorst, 2002);

2. It is noted that in some instances, where indexed distribution patterns mostly correspond to Miller-Bravais indices, no such correspondence is shown by non-indexed columnar plots, as in Figures 6b and 6d. The non-indexed frequencies may resemble bell-shaped distributions similar to those portrayed by French (1998, Figure 4.25).
3. Observation by optical microscopy and TEM of lamellae 1–2 μm wide with ~4–5 μm spacing;
4. Occurrence of multiple intersecting lamellae, and
5. TEM observation of relic non-sub-grain boundaries between segments in optically coherent host quartz (Glikson et al., 2013).

The penetrative lamellae are commonly undulating, wavy and bent, features attributed to deformation, recrystallization and annealing of the host quartz grains, likely representing post-shock centripetal-oriented deformation associated with formation of a central uplift, deformation associated with hydrothermal activity (Naumov, 2002; Pirajno, 2005), or later tectonic events. The planar and sub-planar lamella sets are commonly accompanied by fluid inclusions ("decorated PDFs" - French, 1998) (Figure 5b). Some of the deformation may have been induced by reactivation of fracture and fault networks representing Jurassic (201.7 ± 9.3 Ma), and Cretaceous (~128 to ~86 Ma) tectonic events (Middleton, 2013).

Results of Universal Stage measurements (Table 2; Figure 6a-d) indicate the following:

1. Measurements of in-situ quartz grains within quartz-carbonate veins in arenite indicate a concentration of ~78 per cent of planar features within $\pm 3^{o}$ from the Miller-Bravais indices ({10-13}, {10-12}, {10-11} and {11-21}), diagnostic of shock metamorphism.
2. Due to the common deformation of quartz lamella Universal stage analysis comprised repeated measurements of planar elements within the same planar sets. Frequency distribution plots portray both multiple within-grain measurements as well as the orientations of combined planar sets (Figure 6c).
3. Measurements of planar orientations in quartz grains within arenites confirm the prevalence of Miller-Bravais indices ({10-13}, {10-12}, {11-20}, {2-1-10}) in more than 80 per cent of cases.

The correspondence of the intra-crystalline lamellae with Miller-Bravais indices, the occurrence of multiple intersecting planar features within individual quartz grains and the micron scale (<2μm) intervals of lamellae set {10-12},(Figure 5b) militate for a classification of the quartz lamellae as planar deformation features (PDF) diagnostic of shock

metamorphism. According to French (1998, Table 4.2), the occurrence of the {10-12} planar set suggests pressures in excess of >20 GPa.

Tectonic vs. impact origin of Warburton Basin structures

The origin of the magnetic and seismic tomography anomalies which coincide with the Warburton Basin may be interpreted alternatively in terms of a purely structural or magmatic origin, such as the presence of deep crustal metamorphic or igneous body. Interpretations of penetrative lamellae in quartz as product of possible tectonic–metamorphic processes commonly refer to {0001} planar sets in ignimbrites (Carter et al., 1986) Explosive volcanism may produce Boehm lamellae which mostly display single planar sets (0001) (French and Koeberl, 2010; Vernooij and Langenhorst, 2005). Detrital quartz grains bearing penetrative lamellae in sandstones of unknown provenance (Lyons et al., 1993) may be derived from unidentified impact structures. Quartz lamellae in structural settings not known to be associated with asteroid impact are exemplified by quartzite enclaves in the Rooiberg Felsite, Bushveld Complex (French, 1990). Rhodes (1975) and Elston (2003, 2008) interpreted the Bushveld Complex in terms of a magmatic manifestation of an underlying impact structure. Penetrative quartz lamellae in quartzite xenoliths of the Rooiberg Felsite are marked by fluid inclusions and display a wide scatter of C_{OA}^P_{PE} angles on frequency distribution diagrams (French, 1990, his figures 4 and 5), distinct from frequency distribution patterns corresponding to shock metamorphism-indicative Miller-Bravais indices (French, 1998; French and Koeberl, 2010). Buchanan and Reimold (1996) attributed the lamellae to localized tectonic deformation.

Tectonic and metamorphic deformation of Warburton Basin granitoids, volcanics and sediments may not have reached a degree of penetrative deformation leading to development of metamorphic deformation lamellae in quartz (MDL) as defined by French and Koeberl (2010). Thus, whereas these rocks display extensive fracturing and brecciation, documented in the Warburton East Basin (Sun, 1999), they do not display penetrative deformation which could potentially account for the widespread occurrence of quartz microstructures.

Penetrative quartz lamellae in the Warburton East and Warburton West are in many instances similar to Boehm lamellae and MDLs (Figures 5b, c and d). Boehm quartz lamellae are commonly bent to undulating, may be heavily clouded and are spaced ≥5 μm apart. Mostly only one set of Boehm lamellae or MDL is present in any single quartz grain, whereas two distinct sets are rarely observed (French and Koeberl, 2010; Lyons et al., 1993). Whereas Boehm lamellae may occur in both volcanic and deformed terrains, for example in Finland

(Preston, 1958), Boehm lamella are distinguished from the planar deformation features (PDF) displaying multiple intersecting Miller-Bravais indices and <2 μm spaced lamella.

The occurrence of secondarily re-deformed quartz lamellae in confirmed impact structures, including Vredefort (Grieve et al. 1990, figures 2 and 8), Sudbury (Grieve et al., 2010, figure 6), Manicouagan (Robertson 1975, Dressler 1990, figure 7 and 8), Charlevoix (Trepmann and Spray 2004, figure 1) and Yarrabubba (Glikson, 2013, figure 5.6), allows an interpretation of re-deformed intra-crystalline quartz lamellae in the Warburton Basins in terms of secondary deformation of shock metamorphic lamella (Figures 5c-d). Thus, whereas quartz lamellae within granite and quartz-carbonate veins of the Warburton East and West Basins correspond to Miller-Bravais indices (Figures 6a – c), quartz lamellae in detrital quartz grains show less regular distribution (Figure 6d, e). This suggests (1) that shock metamorphism of the arenite-hosted quartz grains may have been attenuated by the clay matrix which envelope the quartz grains and (2) the detrital quartz grains were subject to more intense re-deformation than granite and vein-hosted quartz grains.

To summarize the evidence for shock metamorphism:

A. Miller-Bravais indices indicative of shock metamorphism
B. Occurrence of multiple sets of intersecting planar quartz lamella
C. Narrow width lamellae ~1–2 μm and inter-lamellar spacing of ~4–5 μm observed by optical microscope and by TEM;
D. TEM evidence for relic optically coherent (non-sub-grain) lamellae (Glikson et al., 2013)
E. Shock metamorphic features correlated with shock levels according to the following scale (French, 1998; Langenhorst, 2002)
    1. Mineral fracturing (0001) and r{10–11} in quartz: 5–7 GPa;
    2. Basal Brazil twins (0001): 8–10 GPa;
    3. PDF ω{10–13}: >10 GPa;
    4. Transformation of quartz to stishovite: 12–15 GPa;
    5. PDF Π{10–12}: >20 GPa;
    6. Transformation of quartz to coesite: >30 GPa.

According to Langenhorst (2002) the appearance of Π{10–12} correlates with >22 GPa pressure, consistent with an interpretation of the Warburton structures as the result of large impact/s. Similar shock pressures have been recorded in Yarrabubba impact structure, Western Australia (Macdonald et al., 2003), Woodleigh impact structure, Western Australia (D=120 km; age ~360 Ma) (Glikson et al., 2005; Uysal et al., 2001, 2002, 2005), the Chesapeake Bay impact structure (D=85 km; age ~35 Ma; Poag et al., 2004).

Bouguer anomaly evidence for low rock densities of 2.64–2.76 g/cm^3 below parts of the Cooper Basin (Meixner et al., 1999, 2000) is consistent with the occurrence of granite cupolas of the Big Lake Granite suite and with hydration and fracturing related to impact, by analogy to the Woodleigh impact structure (Glikson et al., 2005) and Mount Ashmore possible impact structure (Glikson et. al., 2010).

The apparent near-absence of volcanic and sedimentary rocks of upper Devonian to Middle Carboniferous age from both the Warburton East and West Basins (Table 1) may be interpreted alternatively in terms of non-deposition or uplift, erosion and removal of these rock in post-Late Carboniferous times, represented by a major unconformity, defined as seismic Z-Horizon (Boucher, 2001). Such uplift may have occurred during the 'Alice Springs Orogeny' dated by intrusive Upper Carboniferous granitoids (323±5 Ma to 298±4 Ma; Gatehouse et al., 1995) and/or rapid uplift at ~298–295 Ma, leading to exposure and erosion of the Big Lake Granite suite (Gravestock and Jensen-Schmidt, 1998). The uplift, estimated by these authors as ~5000 meters, on the basis of the minimum original depth of emplacement of the Big Lake Granite suite, could potentially represent rebound following a large asteroid impact and would have destroyed the impact crater. An uplift of a ~5 km-high terrain would be eroded in connection with the extensive glaciation represented by the Late Carboniferous to Permian Merimelia and Tirrawarra formations. Reversal of the apparent polar wander path (APWP) during this period suggests major tectonic movements in the end Carboniferous (Klootwijk, 2009). As the age of the Warburton impact/s remains unknown, the stratigraphic position of an ejecta layer cannot as yet be defined.

An impact model involving deep crustal fracturing, suggested by seismic tomography anomalies (Figure 3) may be consistent with the high radiogenic K-U-Th enrichment of the Big Lake Granite suite, possibly due to hydrothermal enrichment in these elements, accounting for the high geothermal gradients of 55–60°C/km in the Nappamerri Trough of the Cooper Basin (Middleton, 1979; Radke, 2009; Wyborn et al., 2004). In these areas temperatures of ~225°C occur at a 5 km depth over an area about 79,000 km2 large and total heat flow of 7.5–10.3 m W m^{-3} are consistent with enrichment of the Big Lake Granite Suite in radiogenic heat-producing elements (Chopra, 2003; McLaren and Dunlap, 2006; Middleton, 1979; Sandiford and McLaren, 2002). A presence of highly radiogenic basement sectors at depth of 3–4 km accounts for upward migration and reconcentration of large ion lithophile elements through the fractured crust, possibly initiated by a hydrothermal cell formed following impact (Naumov, 2002), as observed in the Woodleigh (Glikson et al., 2005), Shoemaker and Yarrabubba impact structures (Pirajno, 2005).

Post-late Carboniferous movements including faulting, fracturing and hydrothermal activity related to Cretaceous extension tectonics are manifest in the Cooper and Galilee

Basins (Middleton et al., 2013, 2014). No evidence of shock metamorphism has been disclosed in these basins (Middleton et al., 2013, 2014; Uysal et al., 2013) although lamellae-bearing detrital quartz grains occur. Nor have shock metamorphic effects been observed in Proterozoic basement rocks and granite intrusions intersected by petroleum drilling holes in Queensland (Tickalara-1, Roseneath-1, Wolgolla-1, Barrolka-2, Balfour-1), which provides further evidence for the unique nature of the Warburton Basin. Reactivation of shock and tectonic-related fracture systems (Waclawik et al., 2008; Clark et al., 2011; Middleton et al., 2013, 2014) may explain the permeable nature of deep crustal structures allowing mantle and crust radiogenic degassing of ^{3}He and CO_2 and heat production (Italiano et al., 2014).

A presence of a deep seated mafic body suggested by gravity and magnetic modelling of the Warburton East Basin (Meixner et al., 1999, 2000) and the Warburton West Basin (Figure 2c) is corroborated by distinct tomography anomalies (Figure 3) under both basins and under the Woodleigh impact structure. Resolution of the geometry of the deep crustal structure of the Warburton Basins must await deep seismic reflection transects, pending which the structures can only be deemed as possible impact structures. An impact on the scale suggested by the Warburton Basin can be expected to have resulted in extensive ejecta fallout units and tsunami deposits, such as is unknown in the Late Carboniferous. A search for ejecta in drill cores from end-Carboniferous sediments of the Bonaparte Basin recovered tuff deposits containing granite fragments (Capuzzo and Bussy, 2001; Gorter et al., 2008). Determination of the age of Warburton impact/s depends on further isotopic age determinations of the Big Lake Granite suite. At the present state of knowledge it is possible the Warburton event constitutes an older, possibly Late Devonian impact cluster, which includes the Woodleigh (~360 Ma; 120 km), Charlevoix (342±15 Ma; 54 km), Alamo Breccia (~370 Ma; ~100 km) (Warme et al., 2002), Siljan (377±2 Ma; 53 km), and Kaluga (360±10 Ma; ~15 km) impact events.

Conclusions

Duane and Reimold (1990) inferred an 800 km-diameter impact structure of Proterozoic age centred under the Simpson Desert, referring to (1) broadly radial central Australia-wide tectonic fault patterns and shear zones, and (2) indirect considerations related to the structural and metamorphic evolution of the Arunta Block in central Australia. This putative Simpson Desert feature overlaps the Warburton West Basin, where we have identified possible shock metamorphic features potentially tectonically modified after formation. However, the present study does not provide evidence for an 800 km impact structure suggested by these authors.

To summarize our observations we report:

(1) The pre-Upper Carboniferous ~450x300 km-large Warburton Basin, north-eastern South Australia, is marked by major magnetic, gravity and low-velocity seismic tomography anomalies, which distinguish the Warburton West Basin from the Warburton East Basin. (2) The >200 km-diameter Warburton East Basin and associated granitoids of the Big Lake Granite suite contain an abundance of quartz grains containing quartz lamellae which correspond to Miller-Bravais indices ({10-13}, {10-12}, {10-11}, {11-21}), diagnostic of shock metamorphism at pressures in excess of 20 GPa (Glikson and Uysal, 2010; Glikson et al., 2013). (3) An investigation of arenites from drill cores in the Warburton West Basin, occupying an area similar in size to the Warburton East Basin (Figures 1 and 2), identifies quartz-carbonate veins and clastic quartz grains containing both pristine and re-deformed quartz lamellae whose orientations correspond to Miller-Bravais indices. (4) Whereas lamellae-bearing clastic quartz could have been re-deposited from earlier rocks, the presence of well-preserved multiple and intersecting lamellae-bearing quartz grains in carbonate-quartz veins suggests in-situ shock metamorphism. (5) Universal stage measurements of Warburton West Basin drill hole samples indicate correspondence of penetrative quartz lamellae with Miller-Bravais indices of {10-12} and {10-13}, correlated with >20 GPa shock pressures. (6) Gravity and magnetic modelling of the Cooper Basin and the Warburton East Basin suggest existence of a high-density (~2.9-3.0 g/cm3) high magnetic susceptibility (SI ~ 0.012-0.037) body at depths below ~6-10 km at the centre of the anomalies. (7) A large magnetic body of SI = 0.030 is modelled below ~10 km in the Warburton West Basin, with a large positive gravity anomaly offset to the north of the magnetic anomaly. (8) Seismic tomography anomalies under both the Warburton East and Warburton West structures indicate likely fracturing of the crust to depths of more than 20 km. (9) Deep seismic transects are required to test the occurrence of mafic magmatic bodies below the centres of the Warburton Basins, possibly representing deep crust and mantle rebound effects and uplift below possible twin impact structures.

Acknowledgements

We are grateful to an anonymous reviewer, an authority in the field of impact science, for comprehensive and in-depth comments and suggestions. John Vickers and Harry Kokonnen

for sample preparations, Alan Whittaker for help with image processing, Elinor Alexander, Rodney Boucher, Prame Chopra, John Gorter, Victor Gostin, Peter Haines, Robert Iasky, Chris Klootwijk, Nick Lemon, Martin Norvick, Hugh O'Neill, Bruce Radke, Erdinc Saygin, John Veevers, Xiaowen Sun and Doone Wyborn for discussions, Les Tucker, David Groom, Karen Groom and Michael Willison of PIRSA for help with sampling of drill cores. We thank PIRSA, Tony Meixner and Bruce Radke for permission to include figures, Elaine Appelbee for drafting several figures. T.P. Mernagh and A.J. Meixner publish with the permission of the Chief Executive Officer, Geoscience Australia.

References

Alexopoulos, J.S., Grieve, R.A.F., Robertson, P.B., 1988. Microscopic lamellar deformation features in quartz: discriminative characteristics of shock-generated varieties. Geology 16, 796–799.

Boucher, R.K., 2001. Nature and origin of the altered zone at the base Cooper Basin unconformity, South Australia. South Australia Department of Primary Industries and Resources Report Book 2001/012.

Buchanan, P.C. Reimold, W.U., 1996. Analysis of Deformation Lamellae in Quartz Grains from the Rooiberg Felsite, Bushveld Complex, South Africa, and Associated Rocks. Lunar and Planetary Science, v. 27, p. 175

Capuzzo, N., Bussy, F., 2001. Syn-sedimentary volcanism in the Late Carboniferous Salvan-Dorenaz Basin, Western Alps. Natura Bresciana 25, 203–211.

Carter, N.J., 1965. Basal quartz deformation lamellae — a criterion for recognition of impactites. American Journal of Science 263, 786–806.

Carter, N.J., 1968. Meteoritic impact and deformation of quartz. Science 160, 526–528.

Carter, N.J., Friedman, M., 1965. Dynamic analysis of deformed quartz and calcite from the Dry Creek Ridge Anticline, Montana. American Journal of Science 263, 747–785.

Carter, N.L., Officer, C.B., Chesnerc, A., Rose, W.I. 1986. Dynamic deformation of volcanic ejecta from the Toba caldera: possible relevance to Cretaceous/Tertiary boundary phenomena. Geology 14, 380–383

Chopra, P., 2003. The search for hot dry rock energy. Preview Australian Society of Exploration Geophysics 107, 34–36.

Clark, D., McPherson, A., Collins, C.D.N., 2011, Australia's seismogenic neotectonic record: a case for heterogeneous intraplate deformation: Geoscience Australia, Record 2011/11, 95 pp.

Dietz, R.S., 1961. Vredefort ring structure: meteorite impact scar? Journal of Geology 69:496–505

Dietz, R.S., 1964. Sudbury structure as an astroblemes. Journal of Geology 72, 412–434

Dressler, B.O., 1990. Shock metamorphic features and their zoning and orientation in the Precambrian rocks of the Manicouagan Structure, Quebec, Canada. Tectonophysics 171, 229-245.

Duane, M.J., Reimold, W.U., 1990. The Simpson Desert Depression – A giant impact basin – Lunar and Planetary Science XXI, 301

Earth Impact Database, Planetary and Space Science Center, 2001 http://www.passc.net/EarthImpactDatabase/index.html

Elston, W. E., 2003. Bushveld Complex, South Africa: impact and plume models reconciled. Large Meteorite Impacts, Lunar and Planetary Science Institute 4032.pdf (abstract)

Elston, W.E., 2008. Proposed Bushveld scenario: Impact, mantle upwelling, meltdown, collapse. Large Meteorite Impacts and Planetary Evolution IV, 3015.pdf (abstract)

Engelhardt, W.V., Bertsch, W., 1969. Shock induced planar deformation structures in quartz from the Ries crater, Germany. Contributions to Mineralogy and Petrology 20, 203-234.

Ferrière, L., Morrow, J.R., Amgaa, T., Koeberl, C., 2009. Systematic study of universal stage measurements of planar deformation features in shocked quartz: implications for statistical significance and representation of results. Meteoritics and Planetary Science 44, 925–940.

French, B.M., 1990. Absence of shock metamorphic effects in the Bushveld Complex, South Africa: results of an intensive search. Tectonophysics 171, 287–301.

French, B.M., 1998. Traces of catastrophe: a handbook of shock-metamorphic effects in terrestrial meteorite impact craters. Lunar and Planetary Institute, Houston, TX, Contribution No 54. 120 pp.

French, B.M., Koeberl, C., 2010. The convincing identification of terrestrial meteorite impact structures: what works, what doesn't, and why. Earth-Science Reviews 98, 123–170.

Gatehouse, C.G., Fanning, C.M., Flint, R.B., 1995. Geochronology of the Big Lake Suite, Warburton Basin, north-east South Australia. Quarterly Geological Notes Geological Survey South Australia 128, 8–16.

Genest, S., Robert, F., Goulet, N., 2011. Otish Basin: discovery of nearly 2.1 GA shocked rocks potentially owning to a D>500 km impact structure, Quebec, Canada. 74th Annual Meeting of the Meteoritical Society: Abstracts, A76.

Geoscience Australia, 2007. AusGeo News December 2007 Issue No. 88 http://www.ga.gov.au/ausgeonews/ausgeonews200712/productnews.jsp

Geoscience Australia, 2009. AusGeo News March 2009 Issue No. 93 http://www.ga.gov.au/ausgeonews/ausgeonews200903/productnews.jsp

Gravestock, D.I., Jensen-Schmidt, B., 1998. Petroleum geology of South Australia: chapter 5: Cooper Basin — structural setting. Report Book 98/9, pp. 47–66.

Glikson, A.Y., Mory, A.J., Iasky, R.P., Pirajno, F., Golding, S.D., Uysal, I.T., 2005. Woodleigh, Southern Carnarvon Basin, Western Australia: history of discovery, Late Devonian age, and geophysical and morphometric evidence for a 120 km diameter impact structure. In: Glikson, A.Y., Haines, P.W. (Eds.), Shoemaker Memorial Issue on the Australian impact record: 1997–2005 update. Australian Journal of Earth Sciences 52, 545–553.

Glikson, A.Y., Uysal, I.T., 2010. Evidence of impact shock metamorphism in basement granitoids, Cooper Basin, South Australia. Australian Geothermal Conference 2010, Adelaide, South Australia.

Glikson, A.Y., Jablonski, D., Westlake, S., 2010. Origin of the Mount Ashmore structural dome, West Bonaparte Basin Timor Sea. Australian Journal of Earth Science 57, 411–430

Glikson, A.Y., Uysal, I.T., Fitz Gerald, J.D., Saygin, E., 2013. Geophysical anomalies and quartz microstructures, Eastern Warburton Basin, North-east South Australia: tectonic or impact shock metamorphic origin? Tectonophysics 589, 57–76.

Glikson, A.Y. , Uysal, I.T., 2013. Geophysical and structural criteria for the identification of buried impact structures, with reference to Australia. Earth Science Reviews, 125, 114–122.

Glikson, A.Y., 2013. The Asteroid Impact Connection of Planetary Evolution. Springer-Briefs, Dordrecht, 150 pp.

Gorter, J.D., 1998. The petroleum potential of Australian Phanerozoic impact structures. Australian Petroleum Exploration Journal 37, 159–186

Gorter, J., Poynter, S.E., Bayford, S.W., Caudullo, A., 2008. Glacially influenced petroleum plays in the Kulshill Group (Late Carboniferous–Early Permian) of the south-eastern Bonaparte Basin, Western Australia. APPEA Journal 2008, 69–98.

Gorter, J.D., Glikson, A.Y., 2012. Talundilly Western Queensland Australia: geophysical and petrological evidence for an 84 km-large impact structure and an early cretaceous impact cluster. Australian Journal of Earth Science 59, 51–73

Gostin, V. A., Haines, P.W., Jenkins, R.J.F., Compston, W., Williams, I.S., 1986. Impact ejecta horizon within late Precambrian shales, Adelaide geosyncline, South Australia. Science 233, 198-200.

Gostin, V.A., Therriault, A.M., 1997. Tookoonooka: a large buried early Cretaceous impact structure in the Eromanga basin of south-western Queensland Australia. Meteoritics and Planetary Science, 32, 593–599.

Grieve, R.A.F., Corderre, J.M., Robertson, P.B., Alexopuolos, J., 1990. Microscopic planar deformation features in quartz of the Vredefort structure: anomalous but still suggestive of an impact origin. Tectonophysics 171, 185–200.

Grieve, R.A.F., Langenhorst, F., Stöffler, D., 1996. Shock metamorphism of quartz in nature and experiment: II. Significance in geoscience. Meteoritics and Planetary Science 31, 6–35.

Grieve, R.A.F., Ames, D.E., Morgan, J.V., Artmieva, N., 2010. The evolution of the Onaping Formation at the Sudbury impact structure.Meteoritics and Planetary Science 45, 159–782.

Hamers, M.F., Drury, M.R., 2011. Scanning electron microscope-cathode-luminescence (SEM-CL) imaging of planar deformation features and tectonic deformation lamellae in quartz. Meteoritics and Planetary Science. Meteoritics and Planetary Science 46, 1814–1831.

Hart , R.J., Cloete M., McDonald, I., Carlson, R.W., Andreoli, M.A.G. 2002. Siderophile-rich inclusions from the Morokweng impact melt sheet, South Africa: possible fragments of a chondritic meteorite. Earth and Planetary Science Letters 198, 49–62.

Hildebrand, A.R., Penfield, G.T., Kring, D.A., Pilkington, M., Camargo, Z.A., Jacobsen, S.B., Boynton, W.V. 1991. A possible Cretaceous-Tertiary boundary impact crater on the Yucatan Peninsula, Mexico. Geology 19, 867–871

Iasky, R.P., Glikson, A.Y., 2005. Gnargoo: a possible 75 km-diameter post-early Permian—pre-Cretaceous buried impact structure Carnarvon basin Western Australia. Australian Journal of Earth Science 52, 577–586

Italiano, F., Yuce, G., Uysal, I.T., Gasparon M., Morelli, G., 2014. A new insight into mantle contribution and basin settings in the Great Artesian Basin, Australia: Evidence from dissolved gas phases in artesian waters. Chemical Geology 378, 75-88

Kamo S.L., Reimold, W.U., Krogh, T.E., Colliston, W.P., 1996. A 2.023 Ga age for the Vredefort impact event and a first report about shock metamorphosed zircons in pseudotachylitic breccias and granophyre. Earth and Planetary Science letters 144, 369–388.

Klootwijk, C., 2009. Australia's controversial Middle–Late Palaeozoic pole path and Gondwana–Laurasia interaction. Australian Journal of Earth Science 56, 273–308.

Langenhorst, F., 2002. Shock metamorphism of some minerals: basic introduction and microstructural observations. Bulletin of the Czech Geological Survey 77 (4), 265–282.

Longley, I.M., 1989. The Talundilly anomaly and its implications for hydrocarbon exploration of Eromanga astroblemes. In: O'Neil, B.J. (Ed.), The Cooper and Eromanga Basins, Australia: Proceedings of the Cooper and Eromanga Basins Conference, Adelaide, 1989, pp. 473–490.

Lyons, J.B., Officer, C.B., Borella, P.E., Lahodynsky, R., 1993. Planar lamellar substructures in quartz. Earth and Planetary Science Letters 119, 431–440.

Macdonald, F.A., Bunting, J.A., Cina, S., 2003. Yarrabubba — a large, deeply eroded impact structure in the Yilgarn Craton, Western Australia. Earth and Planetary Science Letters 213, 235–247.

Masaitis, V.L., 1998. Popigai crater: origin and distribution of diamond-bearing impactites. Meteoritics and Planetary Science 33, 349–359

McLaren, S., Dunlap, W.J., 2006. Use of $^{40}Ar/^{39}Ar$ K-feldspar thermo-chronology in basin thermal history reconstruction: an example from the Big Lake Suite granites, Warburton Basin, South Australia. Basin Research 18, 189–203.

Meixner, A.J., Boucher, R.K., Yeates, A.N., Gunn, P.J., Richardson, L.M., Frears, R.A., 1999. Interpretation of geophysical and geological data sets, Cooper Basin region. South Australia: Australian Geological Survey Organisation, Record, 1999/22.

Meixner, T.J., Gunn, P.J., Boucher, R.K., Yeats, A.N., Murray, L., Yeats, T.N., Richardson, L.M., Freares, R.A., 2000. The nature of the basement to the Cooper Basin region. South Australia Exploration Geophysics 31, 024–032.

Middleton, M.F., 1979. Heat flow in the Moomba, Big lake gas field of the Cooper Basin and implications for hydrocarbon maturation. Bulletin of the Australian Society of Exploration Geophysics 10(2), 149 – 155.

Middleton, A.W, Uysal, I.T., Golding, S.D., Marshalla, V.J., Försterc, H-J, Rhedec, D.. 2013. Integrated geochronology and geochemistry from the Warburton Basin, Australia: Deciphering a thermal and fluid-flow history (Contributions to Mineralogy and Petrology. submitted).

Middleton, A.W., Uysal, I.T., Bryan, S.E., Hall, C.M. , Golding, S.D. (2014) Integrating 40Ar–39Ar, 87Rb–87Sr and 147Sm–143Nd geochronology of authigenic illite to evaluate tectonic reactivation in an intraplate setting, central Australia. Geochimica et Cosmochimica Acta 134, 155–174.

Mory, A.J., Iasky, R.P., Glikson, A.Y., Pirajno, 2000. Woodleigh, Carnarvon Basin, Western Australia: a new 120 km-diameter impact structure. Earth and Planetary Science Letters 177, 119–128.

Naumov, M.V., 2002. Impact generated hydrothermal systems. In: Plado, J., Pesonen, L.J. (Eds.), Impacts in Precambrian Shields. Springer, pp. 117–173.

Preston J., 1958. Quartz lamellae in some Finnish quartzites. Bulletin de la Commission geologique de Finlande 180, 65-78.

Pirajno, F., 2005. Hydrothermal processes associated with meteorite impact structures: evidence from three Australian examples and implications for economic resources. Australian Journal of Earth Science 52 (4/5), 587–606.

Poag, C.W., Koeberl, C., Reimold, W.U., 2004. The Chesapeake Bay crater: geology and geophysics of a late Eocene submarine impact structure. Springer, Berlin, p 522.

Radke, B., 2009. Hydrocarbon and geothermal prospectivity of sedimentary basins in Central Australia Warburton, Cooper, Pedirka, Galilee, Simpson and Eromanga Basins. Geoscience Australia Record 2009/25.

Rhodes, R.C., 1975. New evidence for impact origin of the Bushveld Complex, South Africa. Geology, 3 (10): 549-554

Roberts, D.C., Carroll, P.G., Sayers, J., 1990. The Kalladeina Formation — a Warburton Basin Cambrian carbonate play. The APPEA Journal 30, 166–184.

Robertson, P.B., 1975. Zones of shock metamorphism at the Charlevoix impact structure Quebec. Bulletin Geological Society of America 86, 1630–1638.

Sandiford, M., McLaren, S., 2002. Tectonic feedback and the ordering of heat producing elements within the continental lithosphere. Earth and Planetary Science Letters 204, 133–150.

Saygin, E., Kennett, B.L.N., 2010. Ambient seismic tomography of Australian continent. Tectonophysics 481, 116–125.

Saygin, E., Kennett, B.L.N., 2012. Crustal structure of Australia from ambient seismic noise tomography. Journal of Geophysical Research 117, B01304.

Spray, J.G., Trepmann, C.A., 2006. Shock-induced crystal-plastic deformation and post-shock annealing of quartz. European Journal of Mineralogy 18, 161–173.

Stöffler, D., Langenhorst, F., 1994. Shock metamorphism of quartz in nature and experiment: I. Basic observation and theory. Meteoritics 29, 155–181.

Sun, X., Stuart, W.J., Warren, J.K., 1994. Stratigraphy and sedimentology of Cambro-Ordovician successions, Eastern Warburton Basin, South Australia. PESA Journal 22, 107–111.

Sun, X., 1997. Structural style of the Warburton Basin and control in the Cooper and Eromanga Basins, South Australia. Exploration Geophysics 28, 333–339.

Sun, X., 1998. Prediction of carbonate reservoirs and traps by applying sequence stratigraphy in the Eastern Warburton Basin, South Australia. The APPEA Journal 38, 380–398.

Sun, X., 1999. Fracture analysis of the Eastern Warburton Basin (Early Palaeozoic), South Australia. National Centre for Petroleum Geology and Geophysics, Report Book, 99/00014.

Therriault, A.M., Grieve, R.A.F., Reimold, W.U., 1997. Original size of the Vredefort Structure: implications for the geological evolution of the Witwatersrand Basin. Meteoritics and Planetary Science 32, 71–77.

Trepmann, C., Spray, J.G., 2004. Post-shock crystal plastic processes in quartz from crystalline target rocks of the Charlevoix impact structure. Lunar and Planetary Science XXXV.

Uysal, I.T., Golding, S.D., Glikson, A.Y., Mory, A.J. , Glikson, M., 2001. K–Ar evidence from illitic clays of a Late Devonian age for the 120 km diameter Woodleigh impact structure, southern Carnarvon Basin, Western Australia. Earth and Planetary Science Letters 192, 281–289.

Uysal, I.T., Golding, S.D., Glikson, A.Y., Mory, A.J., Glikson, M., Iasky, R.P., Pirajno, 2002. Reply to "Comment on: 'K–Ar evidence from illitic clays of a Late Devonian age for the 120 km diameter". Earth and Planetary Science Letters 201, 253–260.

Uysal, I.T., Mory, A.Y., Golding, S.D., Bolhar, R., Collerson, K.D., 2005. Clay mineralogical, geochemical and isotopic tracing of the evolution of the Woodleigh impact structure, Southern Carnarvon Basin, Western Australia. Contributions to Mineralogy and Petrology, 149, 576-590.

Uysal, I.T., Ring, U., Middleton, A.W., 2013. Understanding the role of Phanerozoic and active tectonics in generating geothermal resources in central Australia. 22th Annual V.M Goldschmidt Conference, Florence, Italy, August 25-30, p. 2381.

Veevers, J.J., 2009. Mid-Carboniferous Centralian uplift linked by U–Pb zircon chronology to the onset of Australian glaciation and glacio-eustasy. Australian Journal of Earth Sciences 56, 711–717.

Vernooij, M.J.C., Langenhorst, F., 2005. Experimental reproduction of tectonic deformation lamellae in quartz and comparison to shock-induced planar deformation features. Meteoritics and Planetary Science 40, 1353–1361.

Waclawik, V.G.; Lang, S.C.; Krapf, C.B.E., 2008. Fluvial response to tectonic activity in an intra-continental dryland setting: The Neales River, Lake Eyre, Central Australia. Geomorphology, 102 ,179-188.

Warme, J.E., Morgan, M., Kuehner, H.C., 2002, Impact generated carbonate accretionary lapilli in the Late Devonian Alamo Breccia. Catastrophic events and mass extinctions: impacts and beyond. Ed. by Christian Koeberl and Kenneth G. MacLeod, Geological Society of America Special Paper 356, 489-504.

Williams, G.E., 1994. Acraman: A major impact structure from the Neoproterozoic of Australia. Large Meteorite Impacts and Planetary Evolution, Ed. by B. O. Dressler, R. A. F. Grieve, and V. L. Sharpton., Geological Society of America Special Paper 293, pp. 209-224.

Wyborn, D., de Graaf, L., Davidson, S., Hann, S., 2004. Development of Australia's first hot fractured rock (HFR) underground heat exchanger, Cooper Basin, South Australia. In: Boult, P.J., Johns, D.R., Lang, S.C. (Eds.), Eastern Australian Basins Symposium II, ESA Special Publication, pp. 423–430.

Figure captions

Figure 1a. The East and West Warburton Basin, northeast South Australia (Radke, 2009). Known extent of the Warburton Basin on the structure of the pre-Permian 'Z' seismic horizon. The Birdsville Track Ridge divides the Warburton East from the Warburton West Basins.

Figure 1b. A west-east cross section across the Eromanga, Pedirka, Simpson and Warburton (Amadeus) basins, indicating positions of shock metamorphosed quartz grains rocks (full red circles – pre-Z-unconformity rocks; open red circle – post Z-unconformity rocks).

Figure 2a. (1) Total Magnetic Intensity (TMI) of NE South Australia and SW Queensland. (2) Bouguer gravity anomaly of NE South Australia and SW Queensland. Source: Geoscience Australia. EA: East Warburton Basin; WA: West Warburton Basin. The TMI data are based on an airborne magnetic survey conducted for Geoscience Australia by UTS Geophysics Pty Ltd along N-S 400 meters-spaced lines at an above-ground elevation of 60 meters (Geoscience Australia, 2009).

Figure 2b. (1) Total magnetic intensity, reduced to pole: First vertical derivative of the total magnetic intensity): Range: -0.025 to 0.3 nT/m : Contour interval. 0.0025 nT/m. Range, -124 to 296 nT: Magnetic contour interval 10 nT; (2) Bouguer gravity with total magnetic intensity, reduced to pole contours): Range: -360 to 80 gravity units. Modelling by A.J. Meixner.

Figure 2c. East-West and North-South magnetic and gravity sections across the Warburton West geophysical anomaly. Black lines – observations; red and blue lines – models. Modelling by A.J. Meixner.

Figure 3. Tomographic anomalies of the upper crust of the Australian continent. (Saygin and Kennett, 2010). Note the overlap of distinct low group velocity anomalies with the Woodleigh impact structure, Warburton East shock metamorphic terrain and Warburton West terrain.

Figure 4. Relative sedimentary thicknesses, NE South Australia, SW Queensland and SE Northern Territory (Radke, 2009).

Figure 5a. Quartz grains in a quartz-carbonate vein in siltstone, Walkandi-1 core 3122.9 m, Warburton West Basin. (1) top left - A large quartz grain (thick section) in vein within siltstone. scale 500 µm, crossed nicols (CN); (2) bottom left - Corroded quartz grain displaying intra-crystalline lamellae and cross fractures, scale 200 µm, CN; (3) top right - quartz grain showing Π{10–12}, ω{10–13}, s {11-21} planar features, scale 200 µm, CN; (4) bottom right - same as in 5a3 [area outlined in white frame in figure 5a3], scale 50 µm, CN.

Figure 5b. Re-deformed somewhat undulating and clouded lamellae in quartz grains from Walkandi-1 core 3068.2 m and 3067.4 m. Note the presence of cross-cutting lamina. Origin by tectonic origin during formation of a central uplift or alternatively a later discrete tectonic event is undetermined.

Figure 5c. Re-deformed, undulating and clouded lamellae features in quartz grains from Witcherrie-1 1176.5 m core sample. Note the cross cutting lamina at the upper-right grain. Origin by tectonic origin during formation of a central uplift or alternatively a later discrete tectonic event is undetermined.

Figure 5d. Re-deformed, undulating and clouded lamellae in quartz grains from Purni-1 1773.4 m sample and Mokari-1 2031.3 m sample. Origin by tectonic origin during formation of a central uplift or alternatively a later discrete tectonic event is undetermined.

Figure 6a. % Frequency of angles between optic axes of quartz grains (C_{OA}) and the pole of intra-crystalline lamellae features in the same quartz grains ($P_{LAMELLA}$), indexed within ±3 degrees from proximal Miller-Bravais indices for (1) Moomba-1 granite core, Warburton East Basin; (2) McLeod-1 granite core, Warburton East Basin. The frequency distribution plots display multiple intra-grain measurements (solid columns) as well as individual planar sets for each grain (open columns).

Figure 6b. % Frequency at 5 degrees intervals of the angles between optic axes of quartz gains (C_{OA}) to the pole of planar features in the same quartz grains ($P_{LAMELLA}$), based on 62 measurements of quartz lamellae in 9 quartz grains from a quartz-carbonate vein in carbonated siltstones, Warburton Basin. West Walkandi-1 (coordinates: 137.46897E -26.560001); depth 3122.9 m. The frequency distribution plots display multiple intra-grain measurements (solid columns) as well as individual planar sets for each grain (open columns).

Figure 6c. % Frequency angles between optic axes of quartz gains (C_{OA}) to the pole of planar features in the same quartz grains ($P_{LAMELLA}$), indexed within ±3 degrees from proximal Miller-Bravais indices (Π{10–12}, ω{10–13}, s {11-21}, r,z {10-11}), based on 62 measurements of quartz lamellae in 9 quartz grains from a quartz-carbonate vein in carbonated siltstones, Warburton Basin. The frequency distribution plots display multiple intra-grain measurements (solid columns) as well as individual planar sets for each grain (open columns). West Walkandi-1 (coordinates: 137.46897E -26.560001); depth 3122.9 m. The frequency distribution plots display multiple intra-grain measurements (solid columns) as well as individual planar sets for each grain (open columns).

Figure 6d. % Frequency at 5 degrees intervals of the angles between optic axes of quartz gains (C_{OA}) to the pole of planar features in the same quartz grains ($P_{LAMELLA}$), based on 22 measurements of quartz lamellae in 7 quartz grains from quartz grains in quartz arenites and

siltstones from Walkandi-1, Witcherrie-1, Mokari-1 and Purni-1 drill cores, Warburton West Basin. The frequency distribution plots display multiple intra-grain measurements (solid columns) as well as individual planar sets for each grain (open columns).

Figure 6e. % Frequency angles between optic axes of quartz gains (C_{OA}) to the pole of planar features in the same quartz grains ($P_{LAMELLA}$), indexed within ±3 degrees from proximal Miller-Bravais indices (Π{10–12}, ω{10–13}, {11-20}, based on 22 measurements of quartz lamellae in 7 quartz grains from Walkandi-1, Witcherrie-1, Mokari-1 and Purni-1 drill cores, Warburton West Basin. ----------

Table 1.

List of samples from the Macumba-1, Mokari-1, Pandieburra-1, Purni-1, Walkandie-1 and Witcherrie-1 drill holes examined in thin sections

Drill Hole	**Stratigraphy/age**	**Lithology**	**Sample/thin section**
Macumba-1			
2599.6 (meters)	Cambrian-Ordovician		Carbonate-veined cryptocrystalline siltstone
2601.0	Cambrian-Ordovician		Mica and carbonate-bearing siltstone
Mokari-1			
2030.3 (meters)	Post-Carboniferous		
2030.5	Post-Carboniferous		
2031.3	Post-Carboniferous	Partly sandy and silty shale with beds of fine gr. sandstone and siltstone	Fine grained quartz-feldspar arenite. Planar features in quartz
2385.5	NeoProterozoic		Cryptocrystalline carbonate siltstone
Pandieburra-1			
2088.8 (meters)	Rhaetian-Carnbrian		Fine-grained impure quartz arenite
2089.2	"		Fine-grained impure quartz arenite
2140.7	Ordovician		Laminated graphitic quartz and feldspar-bearing siltstone
Purni-1 (meters)			
1773.4	Carboniferous-Permian		Impure fine-grained arenite.

			Planar features in quartz
1773.7	Carboniferous-Permian		Impure fine-grained arenite. Planar features in quartz
1868.9	Cambrian-Ordovician	Silty, dark grey, well bedded, v. pyritic shale with limestone as secondary cement	Cryptocrystalline siltstone
1869.03	"		Cryptocrystalline siltstone
1873.9	"		Cryptocrystalline siltstone
Walkandi-1			
1461.9 (meters)	Post-Ordovician		Near-pure quartzite. Minor lamellae in quartz
2846.9	"		Impure f.g. arenite; quartz grains and interstitial clay-altered feldspar. Planar features in quartz
3067.4	Cambrian-Ordovician	Dullingari Group: Shale, black, pyritic; sandstone, grey, white; mudstone, grey, green.	Impure f.g. arenite; quartz grains and interstitial clay-altered feldspar. Planar features in quartz
3067.7	"		
3068.2	"		Impure fine grained arenite; quartz grains and interstitial clay-altered feldspar. Planar features in quartz
3122.8	Adelaidean	Siltstone	Carbonated siltstone
3122.9	"	"	Cryptocrystalline siltstone veined by quartz and carbonate. Planar features in quartz.
3124.4	"	"	Cryptocrystalline layered siltstone
Witcherie-1			
784.5 (meters)	Devonian	Partly sandy and silty shale, med.-v. coarse gr. poorly sorted sandstone, poorly sorted.	Fine grained feldspar-bearing quartz sandstone
785.9	"		Fine grained Feldspathic greywacke
914.6	"		Fine grained Feldspathic greywacke
921.1	"		Fine grained clay-based feldspathic greywacke

985.6	"		Feldspathic greywacke. Planar features in quartz
1007.5	"		Fine grained feldspathic sandstone
1000.9	"		
1175.5	Cambrian		Fine grained quartzite. Planar features in quartz
1345.5	"		Fine grained quartz-feldspar arenite

Table 2.

(A) Universal stage measurements of angles between C optic axis (C_{OAQZ}) and the pole of intra-crystalline lamellae ($P_{LAMELLA}$) in quartz from Warburton East and Warburton West drill holes, northeast South Australia; (B) lamellae measurements in A indexed to Miller-Bravais planar deformation features.

C_{oa} - C optic axis of quartz
$P_{LAMELLA}$ - Pole to planar deformation feature

Quartz grains	**A**	**B**
Moomba-1 2848.7 m - Quartz grains in Granite (8 quartz grains; 11 planar set measurements)	**Measured angles C_{OA}^$P_{LAMELLA}$ ±3 degrees**	**Indexed angles C_{OA}^$P_{LAMELLA}$ Degrees. NI: Non-indexed**
Grain 1	53	52
Grain 1	26	23
Grain 2	22	23
Grain 3	34	32
Grain 4	35	32
Grain 5	34	32
Grain 6	24	23
Grain 7	22	23
Grain 7	56	NI
Grain 7	35	32
Grain 8	20	23
Moomba-1 2851 m - Quartz grains in Granite (8 quartz grains; 16 planar set measurements)		
Grain 1	67	66
Grain 1	42	NI
Grain 1	64	66
Grain 1	19	NI
Grain 1	47	48
Grain 2	22	23
Grain 2	58	NI
Grain 2	35	32
Grain 3	57	NI
Grain 3	21	23
Grain 3	19	NI
Grain 4	43	NI
Grain 5	0	0

Grain 6	21	23
Grain 7	24	23
Grain 8	35	32
Moomba-1 2851.9m - Quartz grains in Granite (2 quartz grains; 5 planar set measurements)		
Grain 1	24	23
Grain 1	48	48
Grain 1	57	NI
Grain 2	53	52
Grain 2	33	32
Moomba-1 2853.6m - Quartz grains in Granite (2 quartz grains; 9 planar set measurements)		
Grain 1	20	23
Grain 2	58	NI
Grain 2	23	23
Moomba-1 2855.8m - Quartz grains in Granite (4 quartz grains; 9 planar set measurements)		
Grain 1	23	23
Grain 1	17	NI
Grain 1	56	Ni
Grain 1	61	NI
Grain 2	25	23
Grain 3	30	32
Grain 3	75	77
Grain 4	48	48
Grain 4	54	52
Moomba-1 2857.4 m - Quartz grains in Granite (11 quartz grains; 19 planar set measurements)		
Grain 1	23	23
Grain 1	23	23
Grain 1	66	66
Grain 1	24	23
Grain 2	53	66
Grain 2	49	48
Grain 2	64	66
Grain 3	32	32
Grain 4	90	90
Grain 4	86	90
Grain 5	24	23
Grain 6	33	32
Grain 7	33	32
Grain 8	84	82
Grain 9	45	48
Grain 9	48	48
Grain 9	34	32
Grain 10	34	32
Grain 11	80	82
McLeod-1 3745.2 Quartz grains in Granite (2 quartz grains; 2 planar set measurements)		
Grain 1	66	66
Grain 2	30	32
McLeod-1 3745.9 m - Quartz grains in Granite (15 quartz grains; 18 planar set measurements).		
Grain 1	80	82
Grain 2	32	32
Grain 3	33	32
Grain 4	33	32
Grain 5	54	52

Grain 5	34	32
Grain 6	22	23
Grain 7	32	32
Grain 8	64	66
Grain 9	80	82
Grain 10	32	32
Grain 11	35	32
Grain 12	32	32
Grain 13	85	82
Grain 14	59	NI
Grain 15	52	52
Grain 15	85	82
Grain 15	48	48
McLeod-1 3747 m - Quartz grains in granite (4 measurements)		
Grain 1	0	NI
Grain 1	18	NI
Grain 1	12	NI
Grain 1	70	NI
Walkandi-1 3122.9 m - Quartz-carbonate vein (8 grains, 62 measurements)		
Grain 1	27	NI
Grain 1	22	23
Grain 1	21	23
Grain 1	24	23
Grain 1	24	23
Grain 1	23	23
Grain 1	22	23
Grain 1	20	23
Grain 1	20	23
Grain 1	37	37
Grain 1	59	NI
Grain 1	31	32
Grain 1	29	32
Grain 1	32	32
Grain 1	32	32
Grain 1	31	32
Grain 1	29	32
Grain 1	24	23
Grain 1	21	23
Grain 1	19	NI
Grain 1	23	23
Grain 1	19	NI
Grain 1	21	23
Grain 1	69	66
Grain 1	67	66
Grain 1	70	NI
Grain 1	68	66
Grain 1	68	66
Grain 1	68	66
Grain 1	68	66
Grain 1	72	74
Grain 1	61	NI
Grain 2	68	66
Grain 3	21	23
Grain 3	57	NI
Grain 3	58	NI

Grain 3	20	23
Grain 3	19	NI
Grain 3	53	52
Grain 3	54	52
Grain 3	20	23
Grain 3	59	NI
Grain 3	23	23
Grain 3	22	23
Grain 3	23	23
Grain 4	0	0
Grain 4	0	0
Grain 5	50	52
Grain 5	55	52
Grain 5	55	52
Grain 5	18	NI
Grain 5	22	23
Grain 5	20	23
Grain 5	14	NI
Grain 5	22	23
Grain 5	31	32
Grain 6	50	52
Grain 7	90	90
Grain 8	22	23
Grain 8	30	32
Grain 8	32	32
Grain 8	34	32
Walkandi-1 3067.4 m - Quartz grains in arenite (1 grain 7 measurements),		
Grain 1	26	23
Grain 1	34	32
Grain 1	30	32
Grain 1	33	32
Grain 1	28	NI
Grain 1	32	32
Grain 1	31	32
Purni-1 1773.4 m - Quartz grains in arenite (1 grain 8 measurements)		
Grain 1	33	32
Grain 1	32	32
Grain 1	34	32
Grain 1	36	NI
Grain 1	32	32
Grain 1	28	NI
Grain 1	25	23
Grain 1	24	23
Mokari-1 2031.3 m - Quartz grains in arenite (1 grain 3 measurements)		
Grain 1	17	NI
Grain 1	20	23
Grain 1	21	23
Witcherrie-1 985.6 m - Quartz grains in arenite (1 grain 3 measurements)		
Grain 1	90	90
Grain 1	90	90
Grain 1	90	90
Witcherrie-1 1175.5 m - Quartz grains in arenite		
Grain 1	90	90

No. of investigated quartz grains	66	
No of measured sets	167	
No of lamellae sets/grain	2.5 (Av)	
% Lamellae sets relative to number of grains	39%	
C_{OA}^$P_{LAMELLA}$ = 2	2	
C_{OA}^$P_{LAMELLA}$ = 23	46	27%
C_{OA}^$P_{LAMELLA}$ = 32	40	24%
C_{OA}^$P_{LAMELLA}$ = 48	7	4.2%
C_{OA}^$P_{LAMELLA}$ = 52	11	6.6%
C_{OA}^$P_{LAMELLA}$ = 66	14	8.4%
C_{OA}^$P_{LAMELLA}$ = 74	2	1.2%
C_{OA}^$P_{LAMELLA}$ = 82	6	3.6%
C_{OA}^$P_{LAMELLA}$ = 90	7	4.2%
Non-indexed	34	20.4%

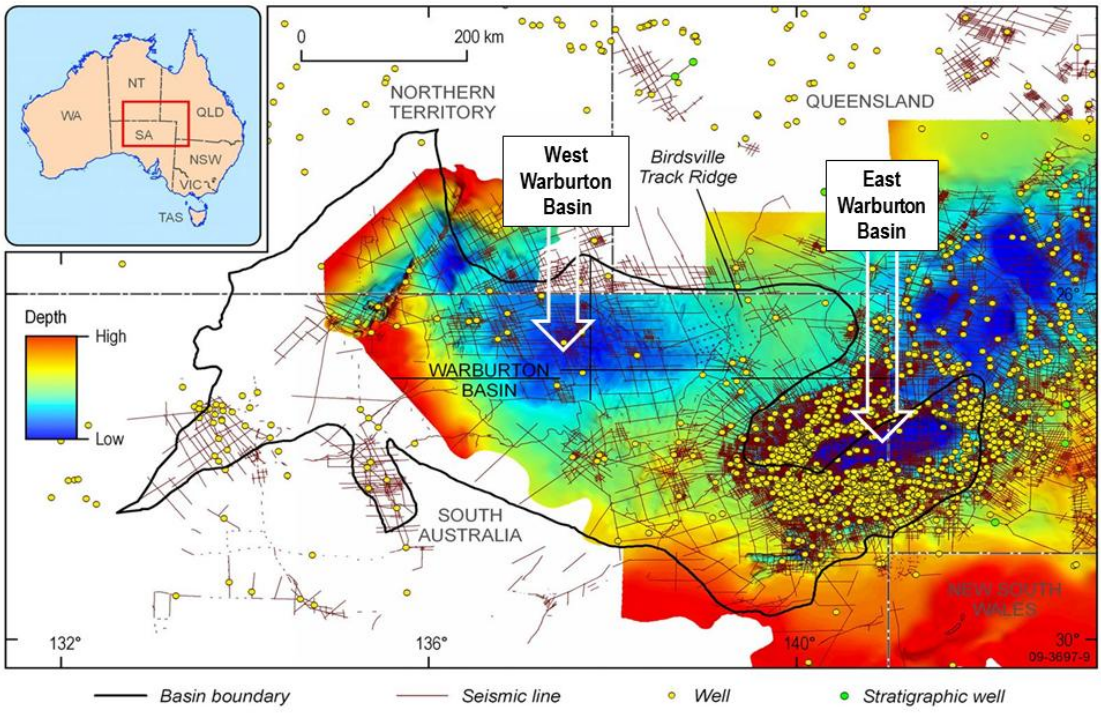
0
200 km
NORTHERN TERRITORY
QUEENSLAND
West Warburton Basin
Birdsville Track Ridge
East Warburton Basin
Depth
High
Low
WARBURTON BASIN
SOUTH AUSTRALIA
NEW SOUTH WALES
132°
136°
140°
20°
30°
09-3697-9
NT
WA
QLD
SA
NSW
VIC
TAS
Basin boundary
Seismic line
Well
Stratigraphic well

Figure 1a

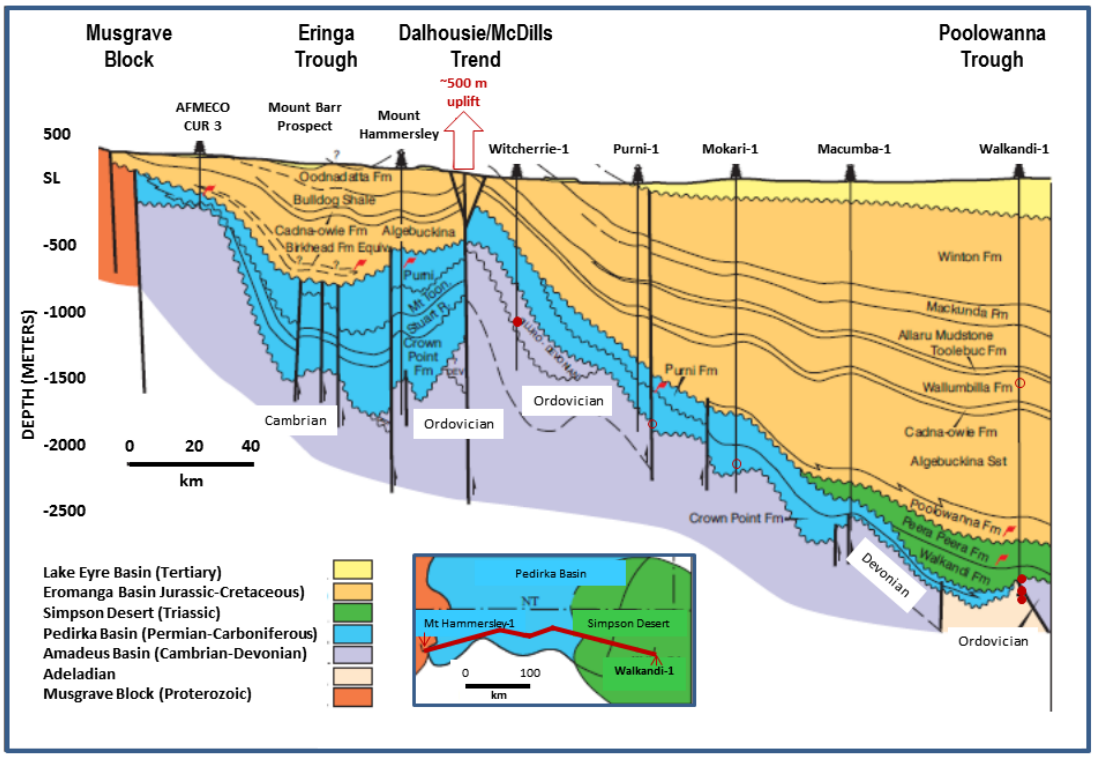
Musgrave Block
Eringa Trough
Dalhousie/McDills Trend
Poolowanna Trough
~500 m uplift
AFMECO CUR 3
Mount Barr Prospect
Mount Hammersley
Witcherrie-1
Purni-1
Mokari-1
Macumba-1
Walkandi-1
DEPTH (METERS)
500
SL
-500
-1000
-1500
-2000
-2500
0 20 40
km
Oodnadatta Fm
Bulldog Shale
Cadna-owie Fm
Birkhead Fm Equiv.
Algebuckina
Purni
Mt Toondina
Stuart Pt
Crown Point Fm
Cambrian
Ordovician
Ordovician
Ordovician
Purni Fm
Crown Point Fm
Devonian
Ordovician
Winton Fm
Mackunda Fm
Allaru Mudstone
Toolebuc Fm
Wallumbilla Fm
Cadna-owie Fm
Algebuckina Sst
Poolowanna Fm
Peera Peera Fm
Walkandi Fm
Lake Eyre Basin (Tertiary)
Eromanga Basin Jurassic-Cretaceous)
Simpson Desert (Triassic)
Pedirka Basin (Permian-Carboniferous)
Amadeus Basin (Cambrian-Devonian)
Adeladian
Musgrave Block (Proterozoic)
Pedirka Basin
NT
Mt Hammersley-1
Simpson Desert
Walkandi-1
0 100
km

Figure 1b

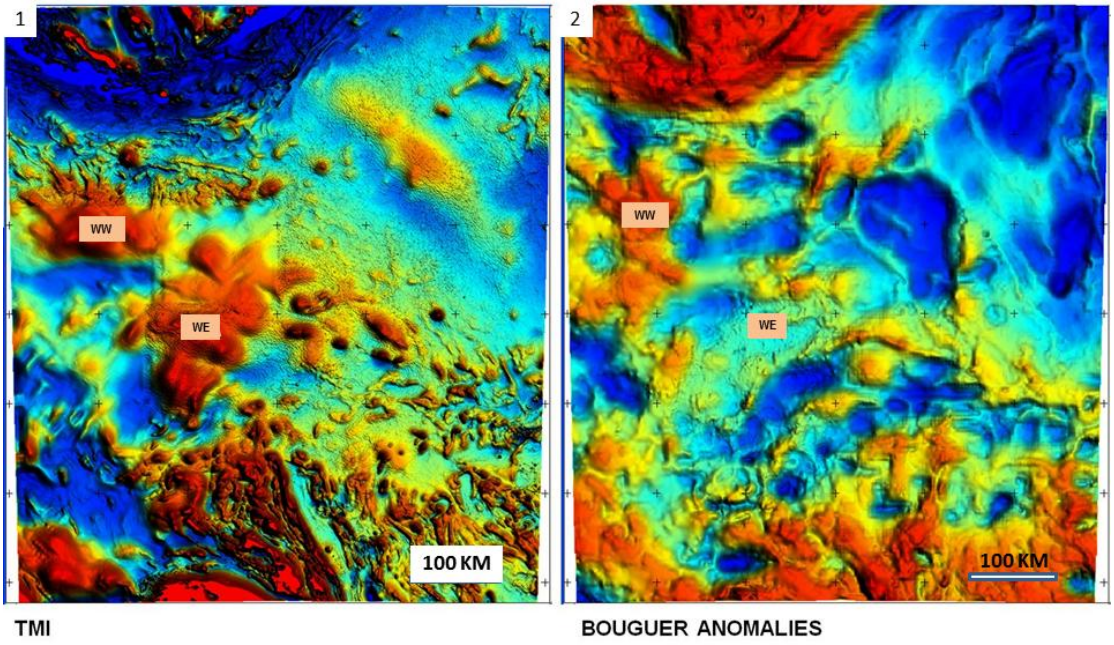

Figure 2a

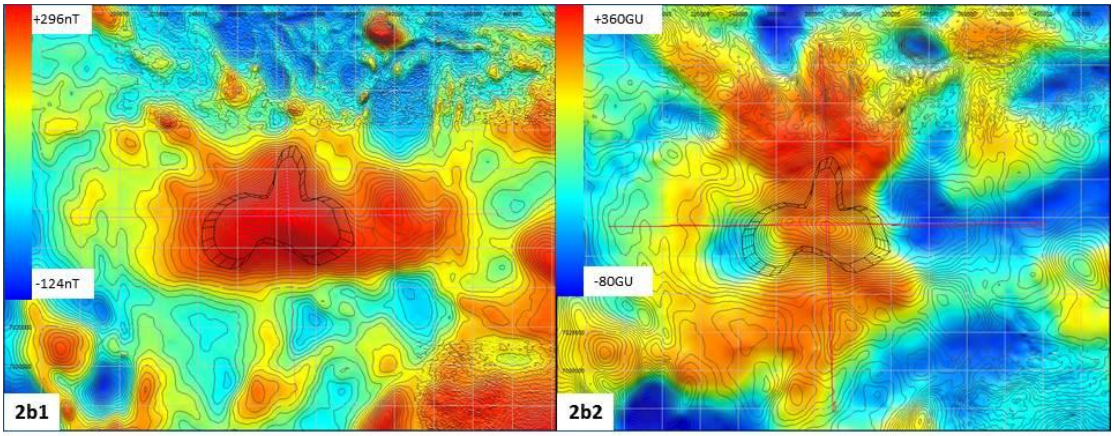

Figure 2b

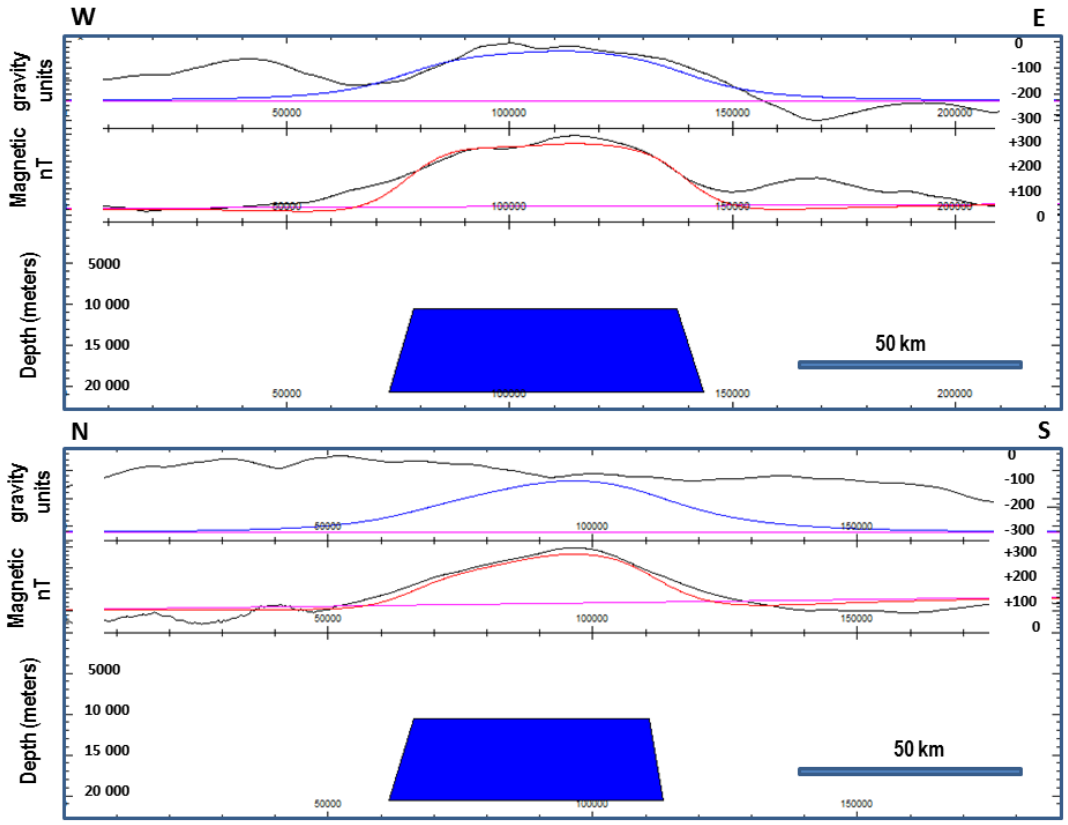
W
E
gravity units
0
-100
-200
-300
Magnetic nT
+300
+200
+100
0
50000
100000
150000
200000
Depth (meters)
5000
10 000
15 000
20 000
50 km
N
S

Figure 2c

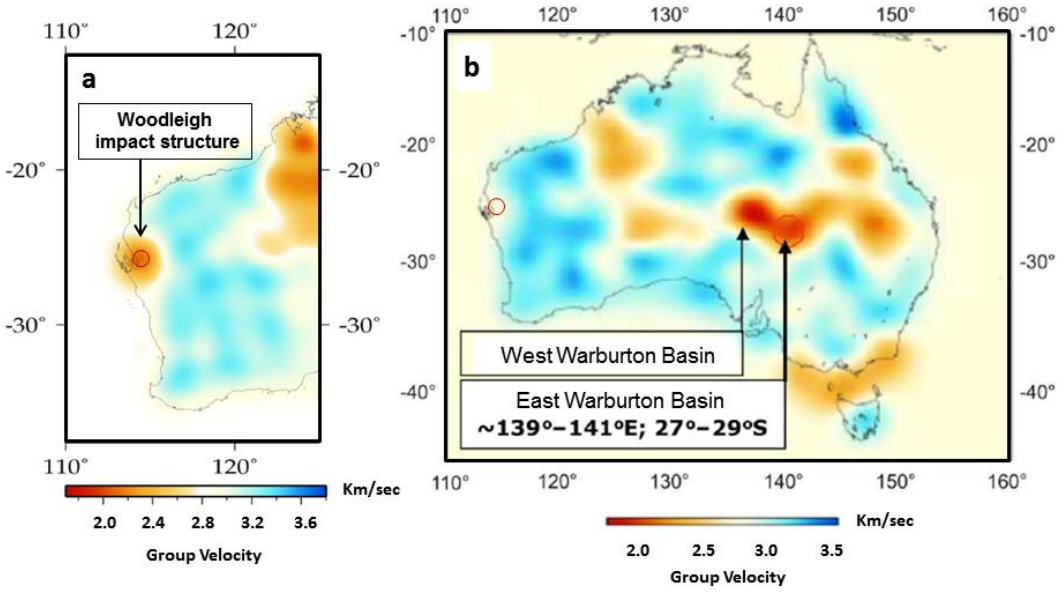
a
Woodleigh
impact structure
110°
120°
-20°
-30°
Km/sec
2.0 2.4 2.8 3.2 3.6
Group Velocity
b
110° 120° 130° 140° 150° 160°
-10°
-20°
-30°
-40°
West Warburton Basin
East Warburton Basin
~139°–141°E; 27°–29°S
Km/sec
2.0 2.5 3.0 3.5
Group Velocity

Figure 3

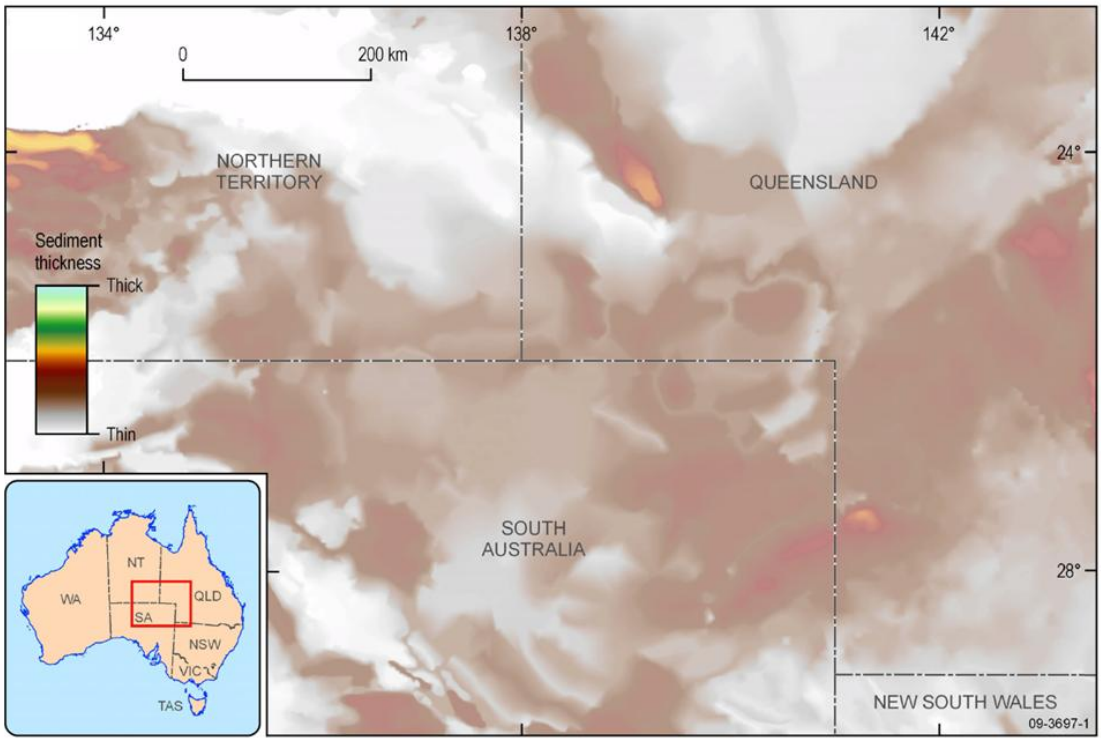
134°
0
200 km
138°
142°
24°
28°
NORTHERN TERRITORY
QUEENSLAND
SOUTH AUSTRALIA
NEW SOUTH WALES
Sediment thickness
Thick
Thin
NT
WA
QLD
SA
NSW
VIC
TAS
09-3697-1

Figure 4

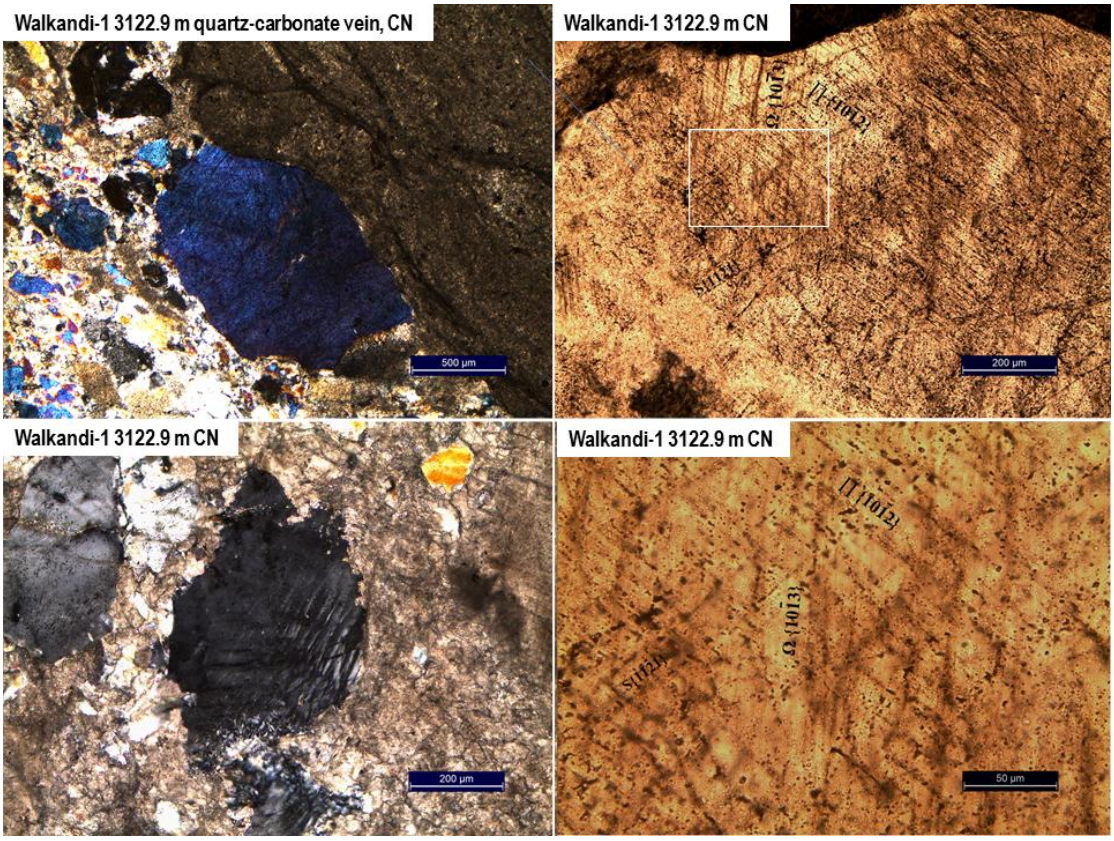
Walkandi-1 3122.9 m quartz-carbonate vein, CN
500 µm
Walkandi-1 3122.9 m CN
200 µm
Walkandi-1 3122.9 m CN
200 µm
Walkandi-1 3122.9 m CN
50 µm

Figure 5a

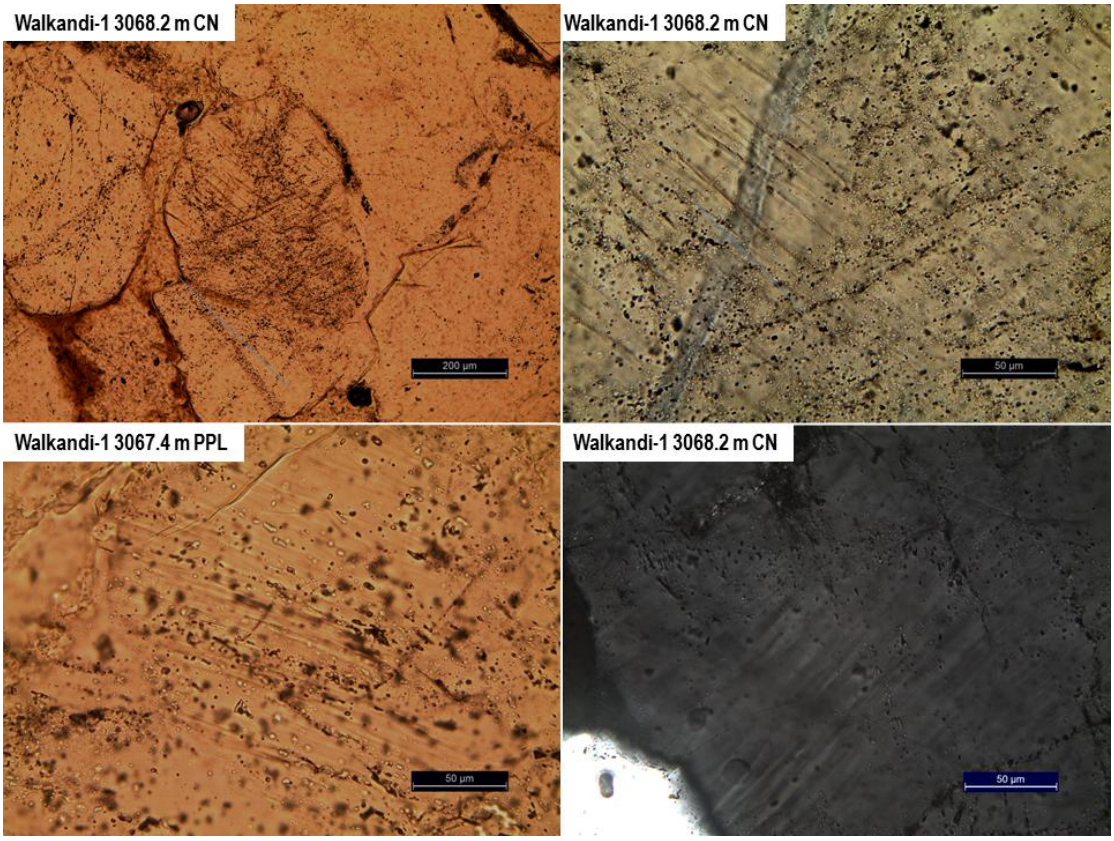
Walkandi-1 3068.2 m CN
200 µm
Walkandi-1 3068.2 m CN
50 µm
Walkandi-1 3067.4 m PPL
50 µm
Walkandi-1 3068.2 m CN
50 µm

Figure 5b

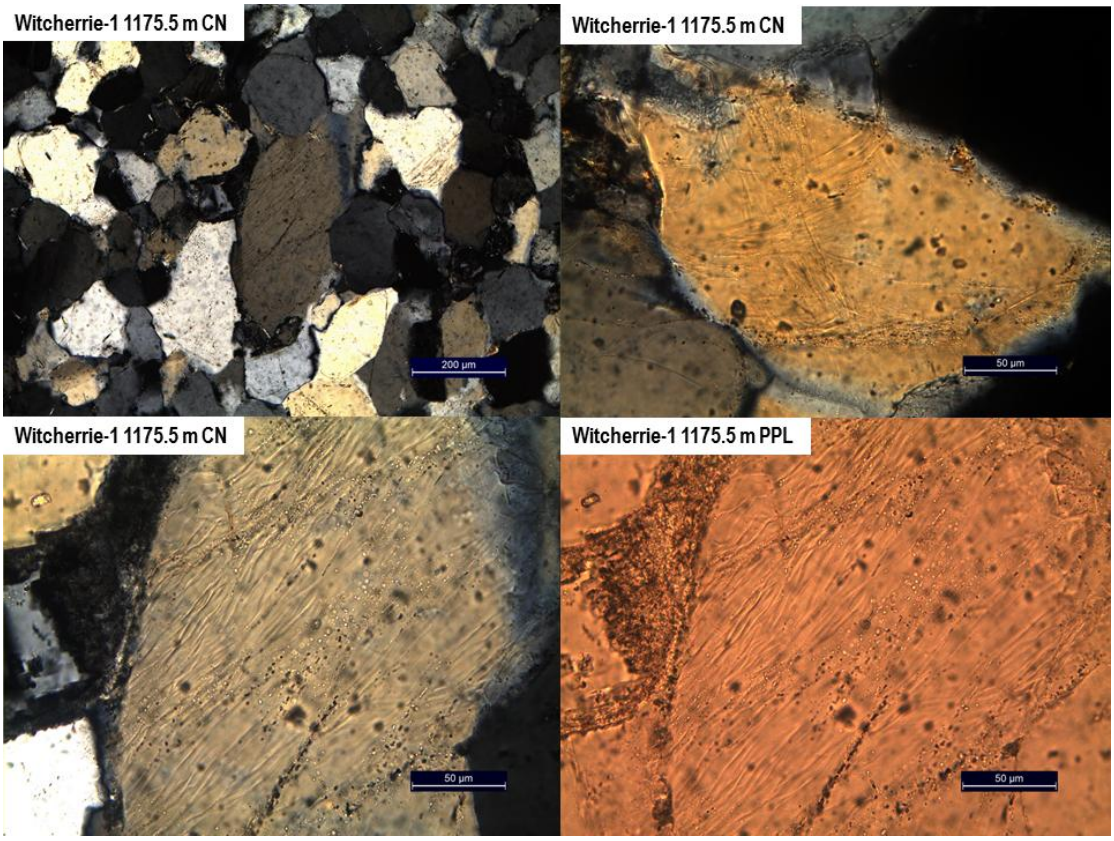
Witcherrie-1 1175.5 m CN
200 µm
Witcherrie-1 1175.5 m CN
50 µm
Witcherrie-1 1175.5 m CN
50 µm
Witcherrie-1 1175.5 m PPL
50 µm

Figure 5c

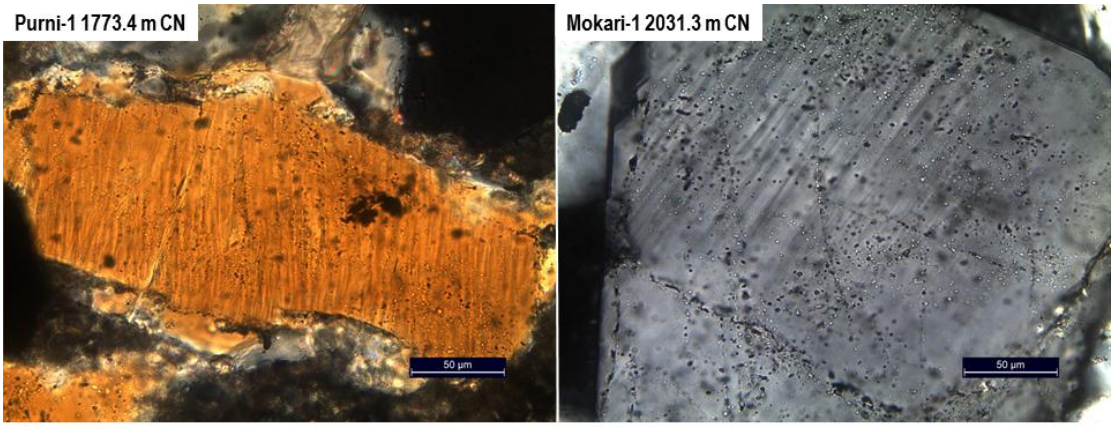

Figure 5d

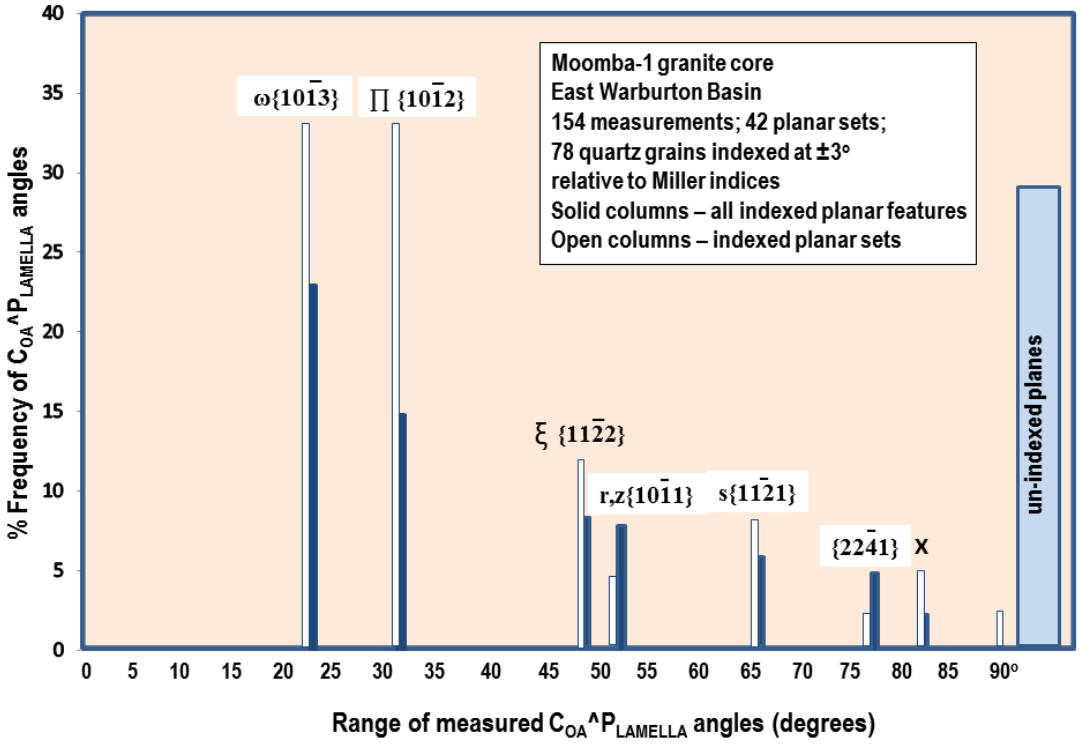
Moomba-1 granite core
East Warburton Basin
154 measurements; 42 planar sets;
78 quartz grains indexed at ±3°
relative to Miller indices
Solid columns – all indexed planar features
Open columns – indexed planar sets
ω{10$\bar{1}$3}
∏ {10$\bar{1}$2}
ξ {11$\bar{2}$2}
r,z{10$\bar{1}$1}
s{11$\bar{2}$1}
{22$\bar{4}$1}
x
un-indexed planes
% Frequency of C_{OA}^$P_{LAMELLA}$ angles
Range of measured C_{OA}^$P_{LAMELLA}$ angles (degrees)
0 5 10 15 20 25 30 35 40 45 50 55 60 65 70 75 80 85 90°
0 5 10 15 20 25 30 35 40

Figure 6a-1

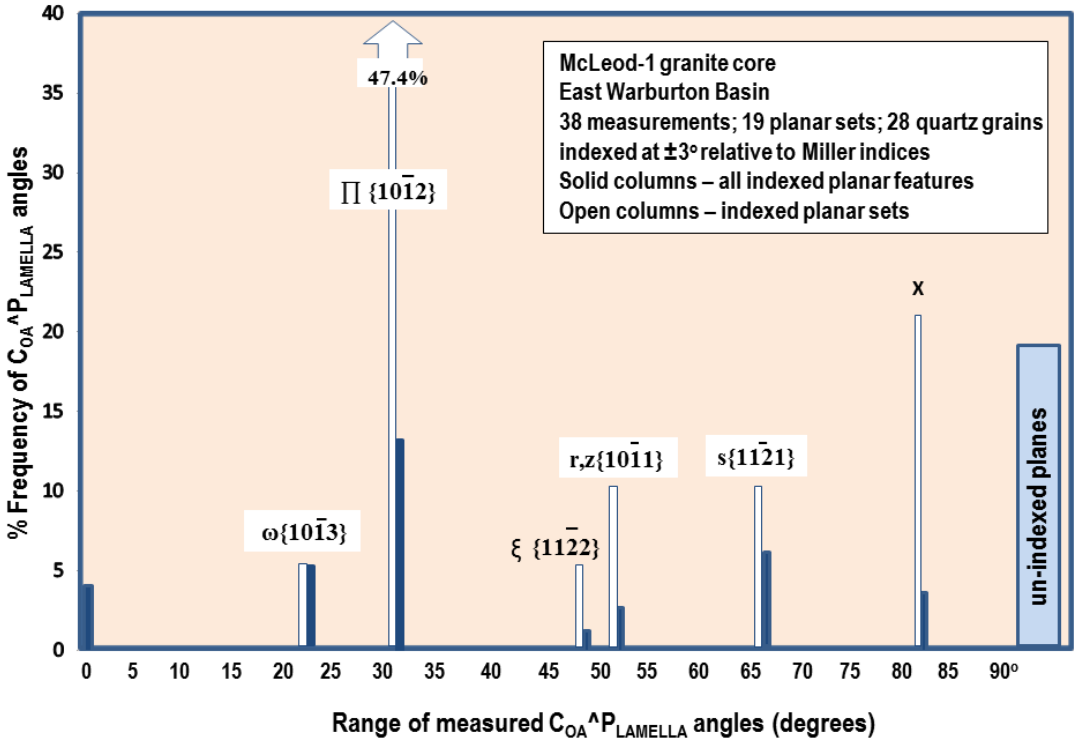
McLeod-1 granite core
East Warburton Basin
38 measurements; 19 planar sets; 28 quartz grains
indexed at ±3° relative to Miller indices
Solid columns – all indexed planar features
Open columns – indexed planar sets
47.4%
∏ {10$\bar{1}$2}
ω{10$\bar{1}$3}
ξ {11$\bar{2}$2}
r,z{10$\bar{1}$1}
s{11$\bar{2}$1}
x
un-indexed planes
% Frequency of C_{OA}^$P_{LAMELLA}$ angles
Range of measured C_{OA}^$P_{LAMELLA}$ angles (degrees)
0 5 10 15 20 25 30 35 40 45 50 55 60 65 70 75 80 85 90°
0 5 10 15 20 25 30 35 40

Figure 6a-2

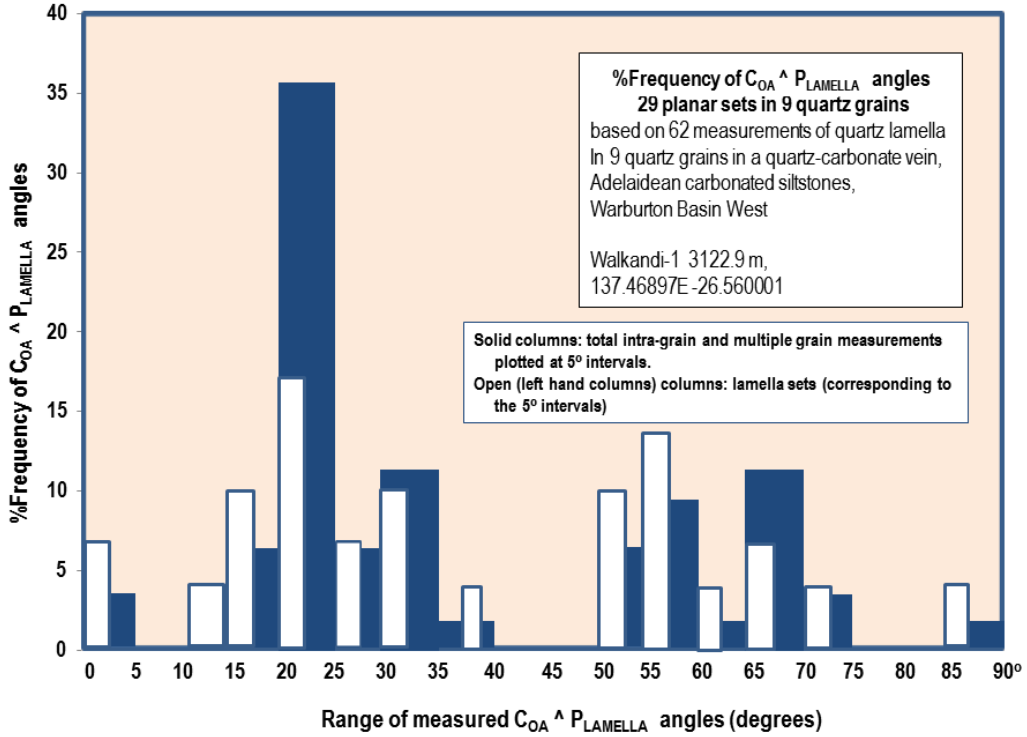
%Frequency of C_{OA} ^ $P_{LAMELLA}$ angles
29 planar sets in 9 quartz grains
based on 62 measurements of quartz lamella
In 9 quartz grains in a quartz-carbonate vein,
Adelaidean carbonated siltstones,
Warburton Basin West
Walkandi-1 3122.9 m,
137.46897E -26.560001
Solid columns: total intra-grain and multiple grain measurements plotted at 5º intervals.
Open (left hand columns) columns: lamella sets (corresponding to the 5º intervals)
%Frequency of C_{OA} ^ $P_{LAMELLA}$ angles
Range of measured C_{OA} ^ $P_{LAMELLA}$ angles (degrees)
0 5 10 15 20 25 30 35 40 45 50 55 60 65 70 75 80 85 90º
0 5 10 15 20 25 30 35 40

Figure 6b

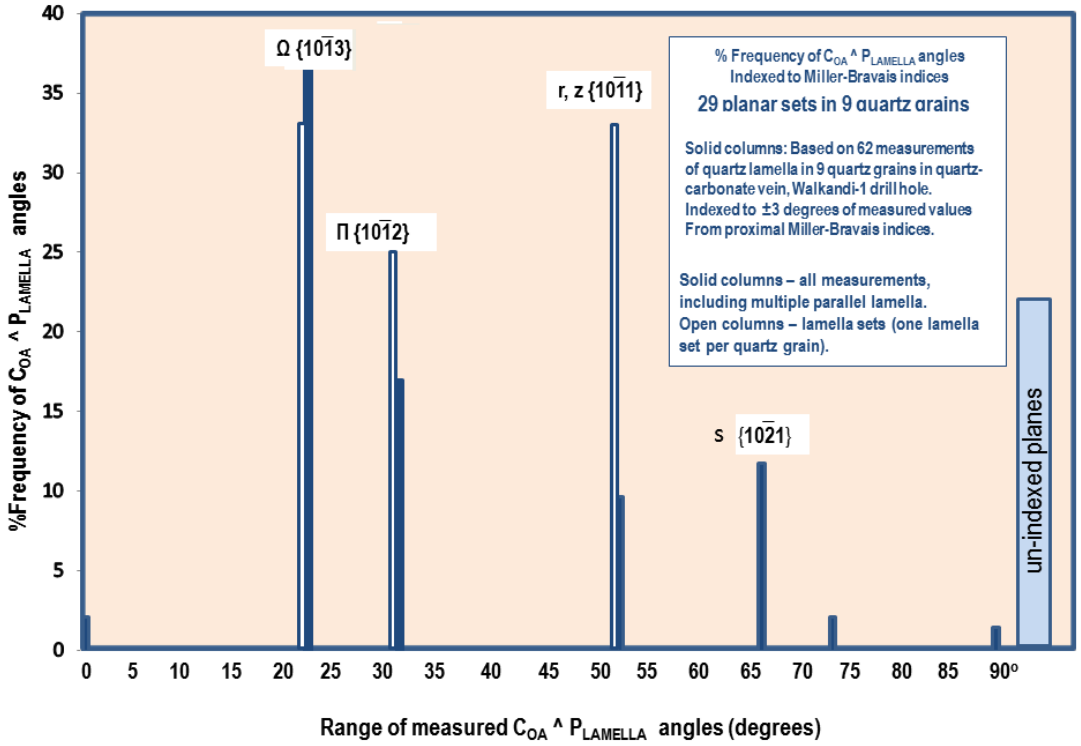
Ω {10$\bar{1}$3}
Π {10$\bar{1}$2}
r, z {10$\bar{1}$1}
s {10$\bar{2}$1}
un-indexed planes
% Frequency of C_{OA} ^ $P_{LAMELLA}$ angles
Indexed to Miller-Bravais indices
29 planar sets in 9 quartz grains
Solid columns: Based on 62 measurements of quartz lamella in 9 quartz grains in quartz-carbonate vein, Walkandi-1 drill hole. Indexed to ±3 degrees of measured values From proximal Miller-Bravais indices.
Solid columns – all measurements, including multiple parallel lamella.
Open columns – lamella sets (one lamella set per quartz grain).
%Frequency of C_{OA} ^ $P_{LAMELLA}$ angles
Range of measured C_{OA} ^ $P_{LAMELLA}$ angles (degrees)
0 5 10 15 20 25 30 35 40 45 50 55 60 65 70 75 80 85 90°

Figure 6c

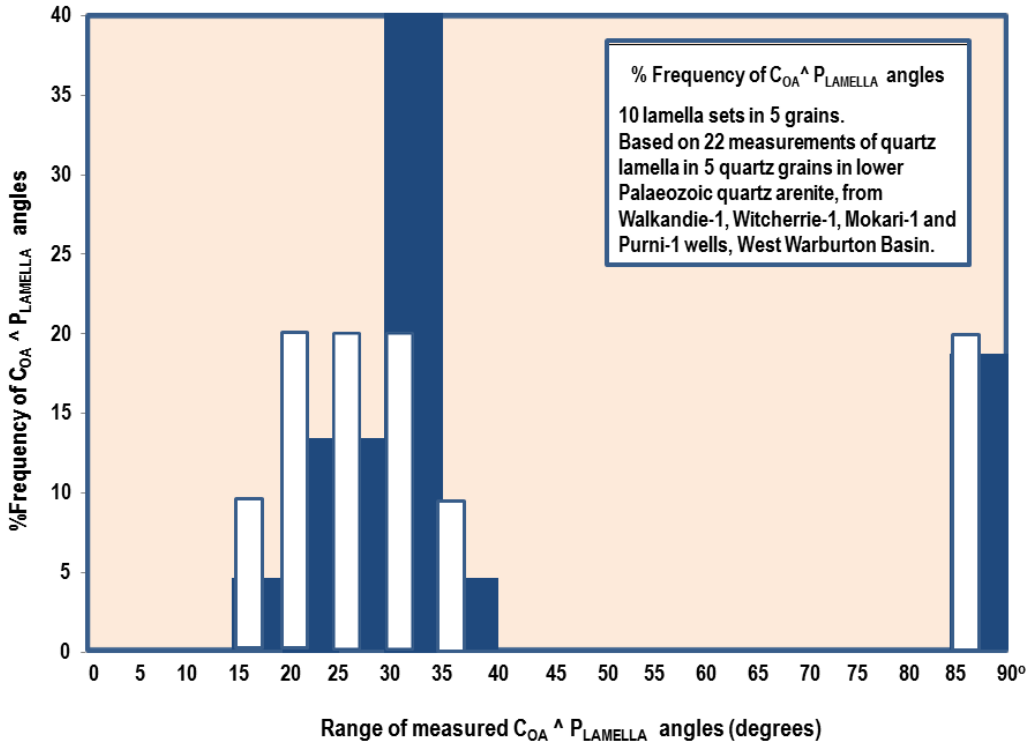
% Frequency of C_{OA} ^ $P_{LAMELLA}$ angles
10 lamella sets in 5 grains.
Based on 22 measurements of quartz lamella in 5 quartz grains in lower Palaeozoic quartz arenite, from Walkandie-1, Witcherrie-1, Mokari-1 and Purni-1 wells, West Warburton Basin.
%Frequency of C_{OA} ^ $P_{LAMELLA}$ angles
Range of measured C_{OA} ^ $P_{LAMELLA}$ angles (degrees)
0
5
10
15
20
25
30
35
40
45
50
55
60
65
70
75
80
85
90°

Figure 6d

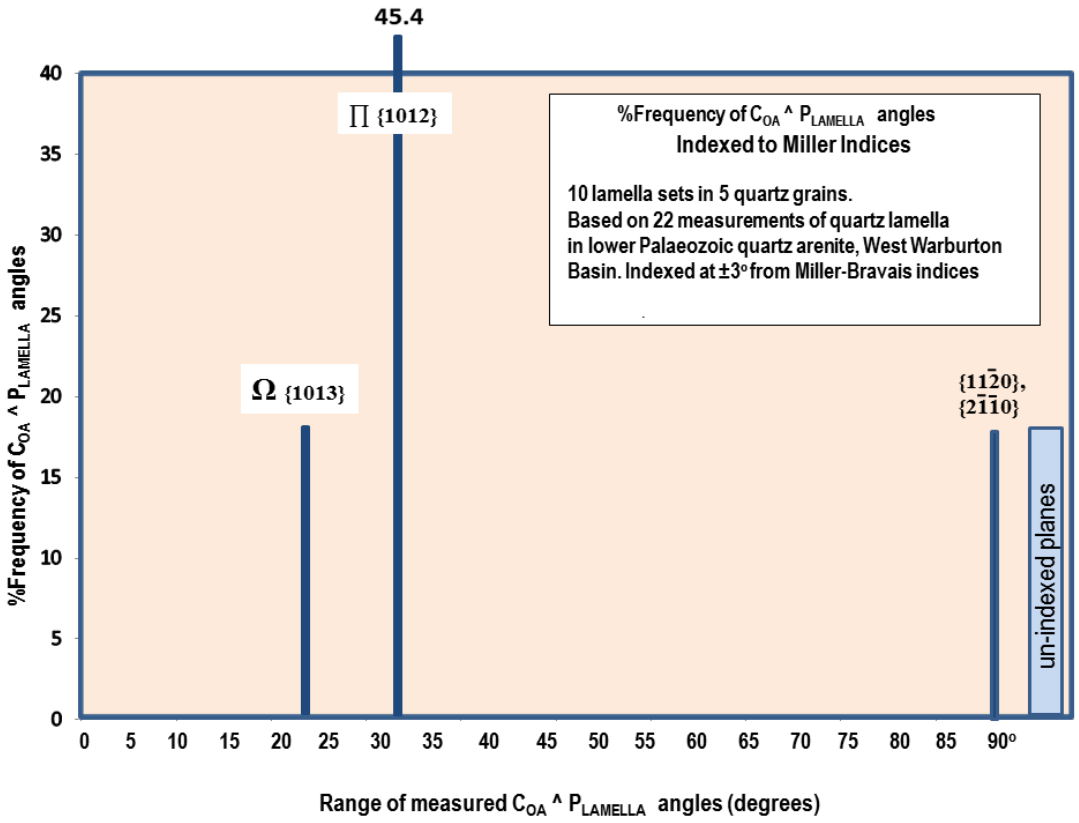
45.4
∏ {1012}
Ω {1013}
{11$\bar{2}$0},
{2$\bar{1}\bar{1}$0}
un-indexed planes
%Frequency of C_{OA} ^ $P_{LAMELLA}$ angles
Indexed to Miller Indices
10 lamella sets in 5 quartz grains.
Based on 22 measurements of quartz lamella
in lower Palaeozoic quartz arenite, West Warburton
Basin. Indexed at ±3° from Miller-Bravais indices
%Frequency of C_{OA} ^ $P_{LAMELLA}$ angles
0 5 10 15 20 25 30 35 40
0 5 10 15 20 25 30 35 40 45 50 55 60 65 70 75 80 85 90°
Range of measured C_{OA} ^ $P_{LAMELLA}$ angles (degrees)

Figure 6e

HIGHLIGHTS

1. The paper reports large buried possible impact structures in central Australia.

2. The structures are marked by deep-seated magnetic and seismic tomography anomalies

3. U-stage and TEM studies of quartz define Miller-Bravais and deformed lamella

4. Missing Devonian to upper Carboniferous strata suggest strong uplift.